https://doi.org/10.5194/egusphere-2026-4499
Preprint. Discussion started: 1 September 2026

Measurement Report: Molecular Dynamics of Organic Aerosol in the Wintertime East China Sea Driven by East Asian Outflows

Hao Li[1], Xiaofei Qin[2], Jian Xu[3], Qianqian Gao[1], Kai Bi[4], Zhaoze Deng[5], Jianguo Liu[6], Haitao Zheng[6], Xiaoyu Ren[4], Xiaofei Wang[1], Congrui Deng[1,7], Kan Huang[1,7,8,9]*

[1]Shanghai Key Laboratory of Air Quality and Environmental Health, National Observations and Research Station for Wetland Ecosystems of the Yangtze Estuary, Department of Environmental Science and Engineering, Fudan University, Shanghai 200433, China

[2]School of Environmental and Municipal Engineering, Qingdao University of Technology, Qingdao, 266520, China

[3]Department of Chemistry, University of Oslo, P.O. 1033 - Blindern, 0315 Oslo, Norway

[4]Beijing Weather Modification Center, Beijing, 100089, China

[5]State Key Laboratory of Atmospheric Environment and Extreme Meteorology, Institute of Atmospheric Physics, Chinese Academy of Sciences, 100029 Beijing, China

[6]Key Lab of Environmental Optics and Technology, Anhui Institute of Optics and Fine Mechanics, Hefei Institutes of Physical Science, Chinese Academy of Sciences, Hefei 230031, China

[7]Institute of Eco-Chongming, No. 20 Cuiniao Road, Chen Jiazhen, Shanghai, 202162, China

[8]Observation and Research Station of Huaniaoshan East China Sea Ocean-Atmosphere Integrated Ecosystem, Ministry of Natural Resources, Shanghai 200136, China

[9]IRDR ICoE on Risk Interconnectivity and Governance on Weather/Climate Extremes Impact and Public Health, Fudan University, Shanghai 200433, China

Correspondence: huangkan@fudan.edu.cn

https://doi.org/10.5194/egusphere-2026-4499
Preprint. Discussion started: 1 September 2026

Abstract

Organic aerosol (OA) represents a significant component in the marine atmosphere, yet its chemical composition and sources remain poorly constrained owing to its relatively sparse observations in coastal regions. This study investigates molecular characteristics and evolution of OA by high-resolution mass spectrometry during winter over the East China Sea. The detected thousands of organic compounds exhibited low O/C ratios (0–0.6) but broad H/C distributions. Over 95% (ESI+) and 60% (ESI-) of detected molecules were highly sensitive to air mass origins, revealing the dynamic interplay between marine and anthropogenic emissions. The CHON subgroup dominated the ESI+ mode (55 – 58%), while the dominant subgroups in the ESI- mode varied with atmospheric processes. The CHON- subgroup fraction surged substantially during pollution episodes, particularly for nitro-aromatics. The CHOS- subgroup was more sensitive to aqueous-phase reactions and facilitated by elevated SO_2/SO_4^{2-} levels, leading to the formation of organosulfate ($O/S \geq 4$). Marine biomarkers persisted across all periods, indicating pronounced resilience of marine emissions even in winter. The bulk volatility increased during polluted periods, particularly for CHON- and CHN+ subgroups, driven by primary emissions and suppressed oxidation. This study demonstrates that continental outflows, atmospheric secondary processes, and persistent marine emissions collectively complicated OA molecular characteristics over the East China Sea.

1. Introduction

Marine aerosol particles, derived from oceanic emissions, contribute more than 50% of natural aerosols globally (Erickson and Duce, 1988), which have legitimately been responsible for a pronounced biological cycle and climate effect (O'dowd and De Leeuw, 2007; Cochran et al., 2017). However, limited understanding of marine aerosols characteristics continues to fuel debate regarding cloud formation and radiative forcing estimates in pristine environments (Rosenfeld et al., 2019). Marine aerosols comprise complex mixtures of sea salt and organic components. These components originated from bubble bursting processes and the oxidation of volatile organic compounds and

https://doi.org/10.5194/egusphere-2026-4499
Preprint. Discussion started: 1 September 2026

primary organic aerosols (Gantt and Meskhidze, 2013; Yu and Li, 2021; Russell et al., 2010; Jiang et al., 2022; Claeys et al., 2010). Globally, marine emissions contribute an estimated 20 $TgCy^{-1}$ of organic aerosols (Albert et al., 2010), which constitute approximately 77% of primary marine aerosol masses (Ovadnevaite et al., 2011), and accounted for over 60% of the organic aerosol mass concentrations in remote marine regions (Brüggemann et al., 2018). Marine organic aerosols enhance cloud droplet number concentrations (CDNC) by 15–100% and act as a critical driver of the marine "biota-cloud-climate" feedback system (O'dowd et al., 2004). Model simulations incorporating ocean-derived organic aerosols show that, under supersaturation conditions of 0.1% (SS = 0.1%), cloud condensation nuclei (CCN) concentrations in the Southern Ocean boundary layer increase by 30 cm^{-3}. This leads to an enhanced annual mean shortwave radiation of -0.36 Wm^{-2}, with average summer cloud radiative forcing reaching -3.5 Wm^{-2} to -4 Wm^{-2} (Burrows et al., 2022), and are comparable in magnitude to the effects of sea salt aerosols. Estimated by Jo et al. (2023), primary marine organic aerosol exerts the highest radiative burden among aerosol types, exceeding that from biomass burning aerosol and anthropogenic primary and secondary organic aerosols. The role of marine organic aerosol is becoming increasingly significant, since their abundance is projected to rise in a warming climate (Weng et al., 2020).

The composition and abundance of marine organic aerosol (OA) exhibit pronounced fluctuations, and are associated with marine plankton activity and carbon pool within surface seawater (O'dowd et al., 2004). Lawler et al. (2020) and Hasenecz et al. (2019) suggested that saccharides constitute 10 - 30% of marine organic fine particle masses, and were emitted from surface seawater. Submicron marine organic aerosols were composed of carbonyl compounds (65 ±12%), alkanes (21 ±9%), amines (6 ± 6%), and carboxylic acids (7 ± 8%) (Frossard et al., 2014). In contrast, dioxylic acids and methanesulfonic acid (MSA) dominate the organic compound in the tropical Atlantic Ocean (Van Pinxteren et al., 2015). This part of SOA formed predominantly from oxidation of dimethyl sulfide (DMS, ~78 %), organic amines (~21 %) and

https://doi.org/10.5194/egusphere-2026-4499
Preprint. Discussion started: 1 September 2026

hydrocarbons (~0.1 %) (Myriokefalitakis et al., 2010). Over the Arctic Ocean, organic aerosols consist mainly of alkanes, organic acids, amines, and organic alcohols, predominantly derived from marine sources (Leaitch et al., 2018). Fu et al. (2013) detected more than 110 organic components based on a global shipping cruise, comfirming primary saccharides as major components, followed by oxidantion products of biogenic volitale organic compounds. In tropical regions, where primary organic aerosol concentrations are relatively low, secondary organic aerosol formed (SOA) from photo-oxidation of VOCs contributes up to 60% of the organic aerosol masses (Brüggemann et al., 2018).

Continental outflows further enhance the contrasts in marine organic aerosols. Previous studies have shown that East Asian outflows caused biomass-burning contributions to OA over the East China Sea, substantially exceeding those from biogenic emissions (Li et al., 2023a), with pronounced regional heterogeneity in OA (Kang et al., 2018). Stable carbon isotope analyses further indicate that continental outflows contribute up to ~60% of OA over the East China Sea (Li et al., 2022a), while an even higher contribution of approximately 70% has been reported over the Arabian Sea (Bikkina et al., 2022). During long-range transport, secondary processes continuously modify OA composition and molecular characteristics (Ajith et al., 2023). For instance, enhanced concentrations of dicarboxylic acids have been attributed to photochemical formation from biomass-burning and combustion-related precursor emissions during transport (Hegde et al., 2022). More importantly, interactions between anthropogenic pollutants and marine VOCs promote the secondary formation of highly hygroscopic organosulfates and organonitrates (Wang et al., 2023; Li et al., 2025; Zhu et al., 2025; Tian et al., 2023), which potentially contribute to CCN formation. Consequently, South Asian continental outflows fundamentally alter the chemical control of CCN activation and cloud droplet formation over the Indian Ocean, with organic-dominated aerosols decoupling CCN from aerosol mass and weakening the relationship between CCN and CDNC in coastal regions compared to the remote ocean (Nair et al., 2024). Critically, minute variations in organic molecular composition

https://doi.org/10.5194/egusphere-2026-4499
Preprint. Discussion started: 1 September 2026

govern >50% of CCN formation (Tröstl et al., 2016; Rejano et al., 2024).

However, tracer-based organic aerosol studies typically quantify only about 4.8 – 5.7% of the total organic mass concentrations (Fu et al., 2013). The complexity involved in chemical processes of OA leads to the coexistence of 10,000 - 100,000 distinct organic compounds in the atmosphere (Allen H. Goldstein and Galbally, 2007), and more than 90% of these species remain uncharacterzied at the molecular level (Franklin et al., 2023; Sandström et al., 2024). Advanced studies enable mechanistic links between molecular components and climate effects. Siegel et al. (2022) proposes a novel and precise approach for predicting CCN based on molecular-level chemical composition observation in the Arctic region. Wan et al. (2020) and Wan et al. (2021) identified the key organic substances driving new particle growth in coastal atmosphere, which are initiated by iodine nucleation from marine biogenic emission. However, due to the inherent chemical complexity of organic aerosols, the set of constants required to characterize their climate properties still needs to be further expanded (Moise et al., 2015).

In recent years, the molecular compositions of organic aerosols across diverse marine regions have been characterized, including the North Atlantic (Gurganus et al., 2015; Wozniak et al., 2014), Northwest Pacific (Bao et al., 2018), Antarctic and Arctic (Ye et al., 2021), and along the eastern coast of China (Sun et al., 2023). Collectively, these studies demonstrate that complex OA molecules exhibited pronounced regional differences in subgroups fraction, molecular characteristics, and specific compound classes. The East China Sea (ECS) serves as a critical natural laboratory for investigating the molecular evolution of organic aerosols, owing to the unique interplay between marine emissions and continental outflows. In this study, we employ high-resolution mass spectrometry to comprehensively characterize the molecular composition and evolution of organic aerosols over the ECS during winter. This season was dominated by distinct air mass types originating from marine regions, northern China, and the Yangtze River Delta (YRD), enabling us to disentangle the influences of different precursors on organic aerosol transformation. Our results advance the

https://doi.org/10.5194/egusphere-2026-4499
Preprint. Discussion started: 1 September 2026

understanding of the complex molecular characteristics of marine organic aerosols under the combined effects of multiple sources and atmospheric processes.

2. Methodology

2.1. Sampling

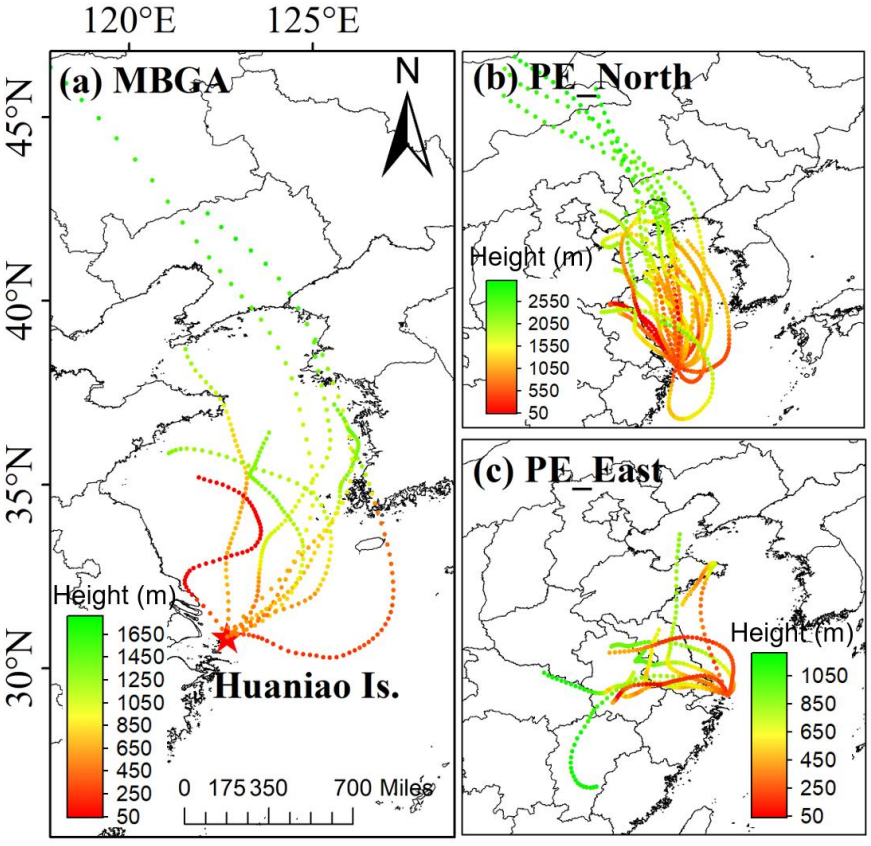

Figure 1. Maps of the observation site (Huaniao Is.), and 48h backward air mass trajectories during three periods, including (a) marine background atmosphere (MBGA), (b) polluted air masses from northern China (PE_North), and (c) polluted air masses from eastern China (PE_East). Backward trajectories are colored by the altitude of air masses.

https://doi.org/10.5194/egusphere-2026-4499
Preprint. Discussion started: 1 September 2026

Field sampling was conducted at Huaniao Island (HNI, 30.85°N, 122.68°E, Figure 1) in January 2019, an offshore island located in the East China Sea and about 80 kilometers away from Shanghai. HNI is an ideal atmospheric background observation site due to negligible local anthropogenic emissions and significant marine emissions (Li et al., 2022b).

$PM_{2.5}$ samples were collected on cellulose filters and quartz filters (Whatman® 41 filters) using high-volume aerosol particles samplers (HY-1000, Hengyuan) at a flow rate of 1.05 m^3/min with a duration of 11 hours (from 08:00 to 17:00 was donated as daytime, and from 18:00 to $07:00^{+1}$ was donated as nighttime). All quartz filters were combusted at 450 ℃ for 4 hours to remove organic residues before sampling, and sampled filters were wrapped in aluminum foil and stored in -18 ℃ to avoid aging of organic components till analysis.

2.2 Chemical Component Analysis

Aerosol chemical components analysis including water-soluble ions and carbonaceous species were conducted by an Ion Chromatograph (IC, DIONEX ICS-3000, Thermo-Fisher) and an Organic Carbon and Elemental Carbon Aerosol Analyzer (OCEC analyzer, RT-3195, Sunset Laboratory, Beaverton, Oregon, USA), and more details were given in our pervious study (Li et al., 2022b).

Organic aerosol analysis at the molecular level was conducted by a high-performance liquid chromatograph (HPLC, 1290 series, Agilent Technologies, USA) coupled with a quadrupole time-of-flight mass spectrometer (Q-ToF MS, Agilent 6564, Agilent Technologies, USA), which was equipped with an electrospray ionization source (ESI). A C18 column (SB-C18, 100 × 3.0 mm, 1.8 μm particle size, Agilent Technologies, USA) was applied for chromatographic separation. The injection volume of each sample was set as 10 μL at a flow rate of 0.4 ml/min. The full scan mode from m/z 50 to 1,700 was employed in both positive and negative modes. Table S1 shows the gradient separation solution and more details about the MS system have been given in Li et al. (2023b).

https://doi.org/10.5194/egusphere-2026-4499
Preprint. Discussion started: 1 September 2026

2.3 Mass Data Processing

All possible formulas were generated within m/z 50 – 800 with a mass tolerance of ±5 ppm, constrained by setting elemental number of atoms in the range of ^{12}C (1−50), ^{1}H (2−100), ^{14}N (0−5), ^{16}O (0−20) and ^{32}S (0−3). The double-bond equivalent (DBEs) of CcHhOoNnSs formula is calculated as follow.

$$\mathrm{DBE} = \frac{2c+2+n-h}{2} \quad (1)$$

The carbon oxidation state (OSc) (Kroll et al., 2011) is calculated by the following equation.

$$\mathrm{OSc} \approx 2O/C - \mathrm{H/C} \quad (2)$$

Where, O/C and H/C are the elemental ratio of oxygen-to-carbon and hydrogen-to-carbon.

The aromaticity equivalent (Xc) was estimated to identified aromatic compounds.

$$X_C = \frac{3(DBE-(p\times o+q\times s))-2}{DBE-(p\times o+q\times s)} \quad (3)$$

p and q represent the ratio of oxygen and sulfur atoms involved in the π-bond structure compounds, which were highly correlated with the categories of detected compounds. p=q=0.5 was chosen for the ESI- mode with sensitivities to compounds containing carboxyl groups, p=q=1 was applied as the possibility of more function groups in the ESI+ mode. o and s represent the number of oxygen or sulfur atoms. Liphatic compounds usually exhibited Xc values lower than 2.50, aromatics with a benzene/naphthalene/anthracene/pyrene core structure usually showed 2.50 ≤ Xc < 2.71, 2.71 ≤ Xc < 2.80, 2.80 ≤ Xc < 2.83, and 2.83 ≤ Xc < 2.92, respectively.

In this study, volatility of organic components was estimated by a two-dimensional volatility basis set (Li et al., 2016; Donahue et al., 2011), i.e., $Log_{10}C_0 = f(n_C, n_O, n_N, n_S)$,

$$Log_{10}C_0 = (n_C^0 - n_C)\times b_C - n_O \times b_O - 2\frac{n_C\times n_O}{n_C+n_O}\times b_{CO} - n_N \times b_N - n_S \times b_S \quad (4)$$

Where C_0 is the saturation mass concentration (μg/m^3), which represents thermodynamic property of the equilibrium distribution of organic compounds between

https://doi.org/10.5194/egusphere-2026-4499
Preprint. Discussion started: 1 September 2026

gas and particle phase. n_C^0 is the reference carbon number; n_C, n_O, n_N, and n_S denote the number of carbon, oxygen, nitrogen and sulfur atoms, respectively. b_C, b_O, b_N, and b_S represent the contribution of each atom to $Log_{10}C_0$, respectively, and b_{CO} is the carbon-oxygen nonideality. According to the function, organic compounds are classified as volatile organic compounds (VOC, $C_0 > 3 \times 10^6$ μg/m^3), intermediate-volatility organic compounds (IVOC, $300 < C_0 < 3 \times 10^6$ μg/m^3), semi-volatile organic compounds (SVOC, $0.3 < C_0 < 300$ μg/m^3), low-volatility organic compounds (LVOC, $3 \times 10^{-4} < C_0 < 0.3$ μg/m^3), and extremely low-volatility organic compounds (ELVOC, $C_0 < 3 \times 10^{-4}$ μg/m^3).

2.4 Auxiliary Data

Temperature (T), relative humidity (RH), wind speed (WS) and wind direction (WD) were measured by an automatic meteorological observation instrument (WXT 520, Vaisala, Finland). Trace gas concentrations, including nitrogen dioxide (NO_2), sulfur dioxide (SO_2) and ozone (O_3) in the transport pathways are obtained from: https://www.aqistudy.cn/historydata/.

Aerosol liquid water content (ALWC) and the bulk aerosol pH were calculated by the thermodynamic equilibrium model, ISORROPIA II (http://isorropia.eas.gatech.edu). The reverse mode and "metastable" state were chosen by using temperature, RH, and aerosol components (Na^+, NH_4^+, K^+, Mg^{2+}, Ca^{2+}, SO_4^{2-}, NO_3^-, Cl^-) as model inputs (Guo et al., 2017; Ge et al., 2019).

3. Results and Discussion

3.1 Contrasting Periods in the Marine Atmosphere

https://doi.org/10.5194/egusphere-2026-4499
Preprint. Discussion started: 1 September 2026

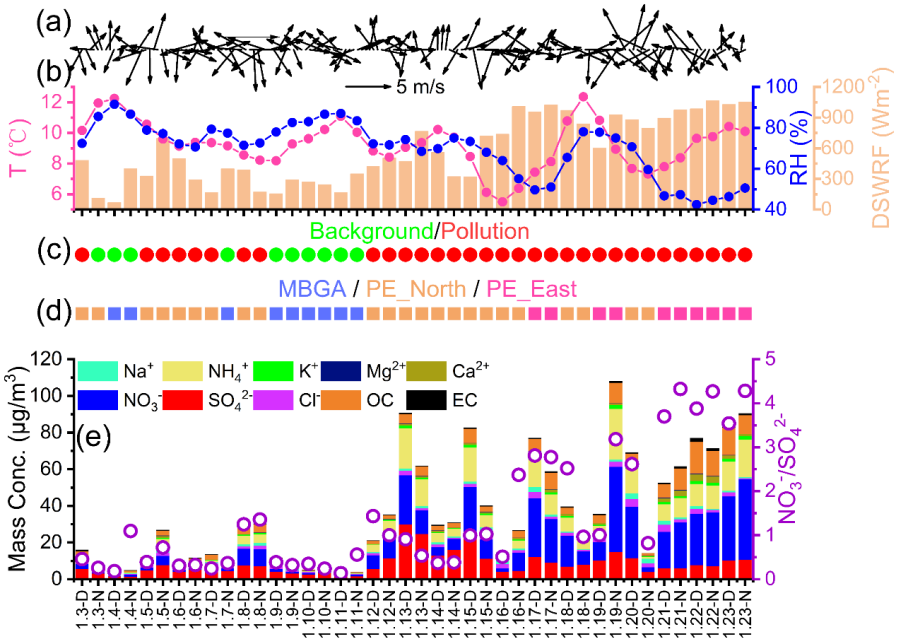

Figure 2. Time series of (a) wind speed and wind direction, (b) temperature, relative humidity and downward short-wave radiation flux, (c) marine background or pollution diagram, (d) categorization of periods based on origins of 48-h backward trajectories, and (e) concentrations of water-soluble ions and carbonaceous aerosols.

Figures 2a&2b show the time series of meteorological parameters during the study period. The weather conditions exhibited moderate temperature (9.3 ± 1.6 ℃) and high relative humidity (70.1 ± 13.1 %). The high wind speed of 6.3 ± 1.8 m/s indicated relatively strong synoptic weather conditions. In this study, the sum of water-soluble inorganic ions (WSIIs) and carbonaceous aerosols larger than 10 μg/m^3 was defined as pollution episodes (PE), and the other days were regarded as marine background atmosphere (MBGA). As displayed in Figures 2c&2e, background atmosphere conditions and pollution periods alternatively appeared. WSIIs during PE reached 38.2

https://doi.org/10.5194/egusphere-2026-4499
Preprint. Discussion started: 1 September 2026

± 24.6 μg/m^3, which was 8.1 times higher than those during MBGA (4.7 ± 1.4 μg/m^3). Secondary inorganic ions, including sulfate, nitrate and ammonium (SNA), accounted for 82.6% and 78.4% during the two periods, respectively. Similarly, carbonaceous aerosols during PE (OC: 5.3 ± 4.3 μg/m^3, EC: 0.7 ± 0.5 μg/m^3) were 7.9 and 4.3 times higher than those during MBGA (OC: 0.7 ± 0.2 μg/m^3, EC: 0.2 ± 0.1 μg/m^3), respectively.

Figures 1a-1c categorize 48-h backward air masses trajectories into three groups. During MBGA, air masses mainly originated from the open ocean. While during PE, air masses can be further grouped into two categories. A significant portion originated from northern China and hovered over a large-scale marine area, which was defined as PE_North. The remaining air masses originated from eastern China and traveled over inland regions, which was defined as PE_East.

During PE_North, sulfate and nitrate were the predominant components with relatively low ratios of NO_3^-/SO_4^{2-} (0.94 ± 0.69) (Figure 2e). As summarized in Table S2, these samples were characterized of higher SO_2, RH, ALWC, and ALWC/$PM_{2.5}$. In contrast, samples during PE_East were dominated by nitrate with significantly higher ratios of NO_3^-/SO_4^{2-} (3.38 ± 0.96). Correspondingly, higher NO_2, O_3, and solar radiation were observed (Table S2). Overall, these differences discussed above provided a distinct contrast for the subsequent analysis of organic aerosol molecular characteristics during three periods.

3.2 Evolution of Organic Aerosols Driven by Continental Outflows

https://doi.org/10.5194/egusphere-2026-4499
Preprint. Discussion started: 1 September 2026

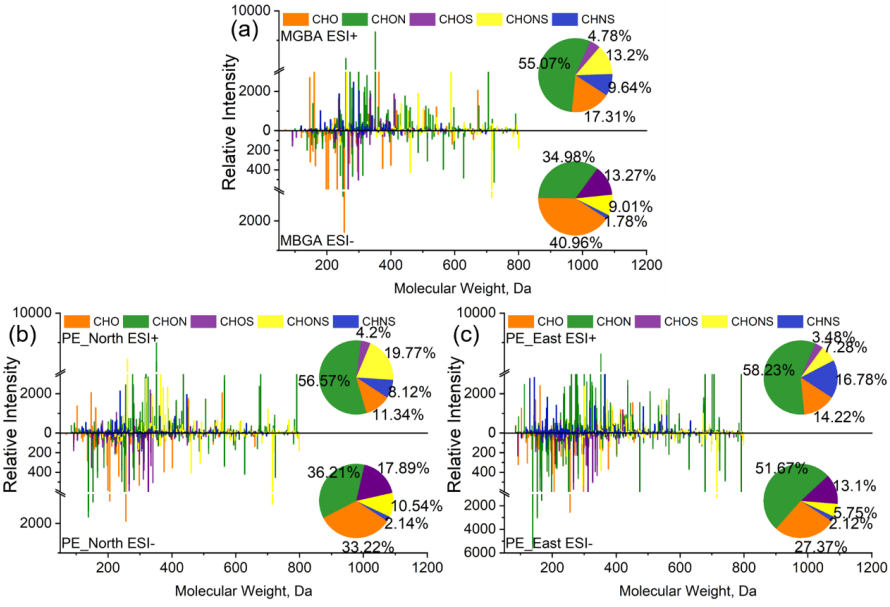

Figure 3. Mass spectra of detected organic components (Note: CHNS* includes CHN, CHS and CHNS compounds) during (a) MBGA, (b) PE_North, and (c) PE_East.

Figures 3a-3c present the mass spectra, normalized relative intensity (RI: peak height/sample volume), and relative abundance fractions of detected organic compounds across the three periods. A total of 569 – 829 and 278 – 383 organic compounds were detected in ESI+ and ESI- modes, respectively. Notably, organic species exhibited significantly higher detection frequency and peak intensity in the ESI+ mode compared to the ESI− mode. This disparity was likely attributed to their enhanced proton affinity and gas-phase basicity, facilitating more efficient ionization and detection under positive ionization conditions (Kiontke et al., 2016; Liigand et al., 2017). The molecular weights (*m/z*) of the detected compounds were predominantly distributed within the 150 - 600 range. The most intense ion peaks occurred within m/z 150 - 300 during MBGA and shifted towards higher molecular weights within *m/z* 150 - 400 during both PE_North and PE_East. The *m/z* distributions observed during PE_North and PE_East were consistent with those reported for biomass burning, coal combustion, and vehicle exhaust emissions (Song et al., 2018; Tang et al., 2020), as

https://doi.org/10.5194/egusphere-2026-4499
Preprint. Discussion started: 1 September 2026

well as in ambient aerosols and cloud water (Bianco et al., 2018; Sun et al., 2021; Zhang et al., 2024).

CHON+ compounds constituted the dominant subgroup in the ESI+ mode across all periods, accounting for 55 – 58% of total relative intensity (Figures 3a-3c). CHO+ (17.3%) represented the second-most abundant subgroup, followed sequentially by CHONS+ (13.2%), CHNS*+ (9.64%), and CHOS+ (4.78%) during MBGA. CHONS+ contributions (19.8%) exceeded CHO+ (11.3%), while CHNS*+ (8.12%) and CHOS+ (4.20%) showed minor reductions during PE_North. CHNS*+ abundance (16.8%) surpassed CHO+ (14.2%), accompanying with further declined CHONS+ (7.28%) and CHOS+ (3.48%) during PE_East.

In the ESI- mode, CHO- compounds dominated (41.0%), followed by CHON- (35.0%), CHOS- (13.3%), CHONS- (9.01%), and CHNS- (1.78%) during MBGA. The contribution of CHON- reached 36.2% during PE_North and substantially increased to 51.7% during PE_East. Concurrently, PE_North displayed elevated CHOS- (17.9%) and CHONS- (10.5%) relative to both MBGA (CHOS-: 13.3%; CHONS-: 9.01%) and PE_East (CHOS-: 13.1%; CHONS-: 5.75%) conditions. This study shows that ESI+ subgroup distributions aligned with the observations in urban areas such as Beijing and Shanghai, however, the ESI- mode revealed a distinctive enhancement in CHON- components relative to CHO- and CHOS- components (Zhang et al., 2024).

The relative compositional variations across different periods likely resulted from synergistic interactions between emission sources and atmospheric chemical processes under distinct air mass transport regimes. Protonated compounds, including amino acids, amines, amides, and their oxidation/fragmentation products, not only exhibited more detection sensitivity in the ESI+ mode due to ionization mechanisms (Lin et al., 2012), but also abundantly presented in aerosols from various sources, which potentially explained the consistent CHON+ proportions (55-58%) observed across all periods. During MBGA when air masses originated from the open ocean (Figure 1a), organic aerosols derived predominantly from direct marine emissions, where biological consumption and photochemistry degradation (Wu et al., 2023) selectively enriched

https://doi.org/10.5194/egusphere-2026-4499
Preprint. Discussion started: 1 September 2026

CHO-dominated dissolved organic matters such as saccharides, organic acids, and polyphenols in surface waters (Ji et al., 2024). CHOS and CHONS compounds accumulated predominantly in eutrophic or terrestrially influenced regions through riverine inputs, anthropogenic pollutant transport, and episodic biological blooms (Wang et al., 2022), evidenced by sulfur-containing DOM from terrestrial runoff and aquacultural activities in coastal seas of China (Wang et al., 2018a; Guo et al., 2021), and enhanced sulfur-containing compounds formation and emissions during algal blooms (especially dimethyl sulfide, DMS) (Wang et al., 2022).

PE_North reflected terrestrial-marine coupling, i.e., anthropogenic pollutants transported over the ocean (Figure 1b), directly contributing CHON, CHONS and CHOS species, and providing abundant sulfur-containing and nitrogen-containing precursors that facilitated aqueous-phase formation of these subgroups. PE_East demonstrated substantial regional influences (Figure 1c), where vehicle emissions, biomass burning (evidenced by peak K^+ (1.37 μg/m^3) and NO_2 (60.1 μg/m^3)) and NOx-driven photochemistry dominated the evolution of organic compounds, particularly for the markable increase of CHON- and CHN+ compounds (Tang et al., 2020). Zhang et al. (2024) documented higher abundances of CHOS and CHONS compounds relative to CHON compounds in urban Beijing and Shanghai, whereas marine studies revealed contrasting patterns. Bao et al. (2018) and Wozniak et al. (2014) reported substantially higher fractions of CHO subgroups (39-59% in the Northwest Pacific; 26-79% in the North Atlantic), with increasing S-containing subgroups and CHON compounds and decreasing CHO compounds near continental sources. This divergence stemmed from selective aerosolization processes where CHO compounds (e.g., saccharides, alcohols, organic acids) exhibited preferential enrichment in sea spray aerosols (Jayarathne et al., 2016). Conversely, marine-derived CHOS/CHONS compounds were characterized by higher oxidation states and polarity (Melendez-Perez et al., 2018), which might reduce the enrichment efficiency in sea spray aerosols relative to their combustion-derived counterparts. This mechanistic distinction likely accounted another reason for the lower CHOS and CHONS fractions observed in this study compared to urban observations

https://doi.org/10.5194/egusphere-2026-4499
Preprint. Discussion started: 1 September 2026

and coastal ship measurements.

3.3 Variations of Molecular Characteristics of Organic Aerosols

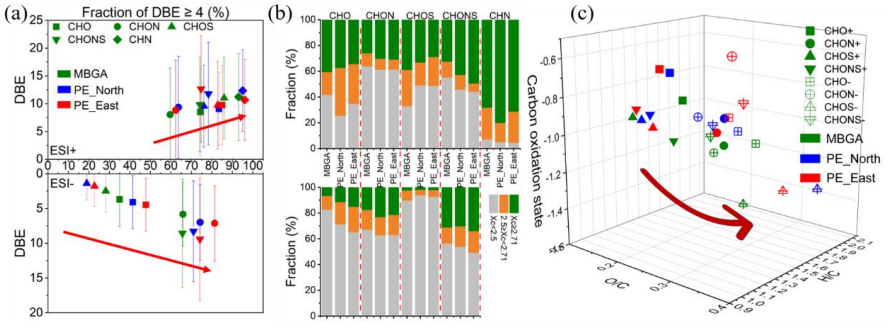

Figure 4. Comparison of (a) DBE, (b) fractions of aromatic compounds for ESI+ (upper) and ESI- (bottom) mode, and (c) mean O/C versus H/C during the three periods.

Figure 4 and Table S3 present bulk molecular characteristics of organic species detected in both ESI+ and ESI- modes. The mean DBE of all subgroups (except CHOS) exhibited progressive increase with pollution levels, accompanied by elevated proportions of compounds with DBE ≥ 4 during PE_North and PE_East relative to MBGA (Figure 4a). These indicated enhanced molecular unsaturation in polluted atmospheres, which was consistently observed in heavily polluted urban areas during winter (Zhang et al., 2024; Wang et al., 2017). Figure 4b and Table S3reveal decreased contributions from non-aromatic compounds (Xc < 2.5) alongside increased proportions of monoaromatics (2.5 ≤ Xc < 2.71) and polycyclic aromatics (Xc ≥ 2.71) (Figure S1, Table S4). Such signatures originated primarily from incomplete combustion sources, i.e., coal pyrolysis under oxygen-deficient conditions release abundant high-DBE compounds including polycyclic aromatic hydrocarbons (PAHs) and tar species, and refractory materials from biomass burning as well (Dong et al., 2012). Besides, abundant acidic species (nitrate and sulfate) may enhance acid-catalyzed carbonyl condensation and oligomerization processes (Dong et al., 2012; Jang et al., 2003), and promoted the formation of highly functionalized compounds

https://doi.org/10.5194/egusphere-2026-4499
Preprint. Discussion started: 1 September 2026

such as nitro-aromatics (Wang et al., 2019), which collectively drove an overall increase in molecular unsaturation.

Figures S2a-S2f display the van Krevelen diagrams (Kim et al., 2003; Heaton et al., 2009) of detected molecular compositions during the three periods. Organic molecules with low O/C ratios (0 – 0.6) constituted a substantial portion of the total organic molecular species, but exhibited a broad H/C distribution (< 2.5). Oligomeric OA components with high DBE values clustered in the center of the van Krevelen diagrams (H:C ~ 1.5, O:C ~ 0.6). Highly oxidized oligomers (O:C > 1) were mainly detected in the ESI+ mode with minor quantities, and only vanishing part of them can be found in the ESI- mode. Figure 4c summarizes the three-dimensional distribution of O/C, H/C, and OSc. During MBGA, organic molecular characteristics were dominated by low-oxygen molecules exhibiting lower O/C and OSc. During PE_North and PE_East, in both ESI+ and ESI- modes, the average O/C and OSc showed an overall increasing trend, while H/C decreased significantly (except for CHOS-, Table S3). This corresponded to the aforementioned increase in the types and abundance of organic species with high unsaturation and the increased proportion of potentially aromatic compounds (Figure S1 and Table S4). Furthermore, this significant decrease in H/C was accompanied by a slight increase in OSc (except for CHON-), which was different from the synchronous rise in O/C, H/C, and OSc reported in secondary-process-dominated regions (Zhang et al., 2025). For CHON- compounds, the O/C and OSc values significantly increased from 0.23 ± 0.20 and -1.14 ± 0.74 during MBGA to 0.25±0.17 and -0.90 ± 0.71 during PE_North, and 0.34 ± 0.22 and -0.52 ± 0.80 during PE_East, respectively. The fraction of CHON- compounds characterized by O/N ≥ 3 also elevated from 24.7% to 29.6% and 46.7% (Table S3), indicating that more CHON- compounds possessed at least one nitro ($-NO_2$) or nitrooxy ($-NO_3$) functional group, and can be classified as oxidized nitrogen-containing compounds. Furthermore, the excess oxygen atoms beyond the $-NO_2$ functional group in these CHON- compounds suggested the presence of additional oxygenated functional groups, such as hydroxyl groups (-OH).

Both CHOS+ and CHOS- compounds exhibited significantly higher DBE during

https://doi.org/10.5194/egusphere-2026-4499
Preprint. Discussion started: 1 September 2026

MBGA compared to the two pollution episodes (Figure 4a), with PE_North showing slightly lower values than PE_East. CHOS+ molecules demonstrated notably high average DBE, with over 50% containing at least one aromatic ring structure ($Xc \geq 2.5$, Figure 4b). Meanwhile, CHOS+ compounds maintained nearly identical O/C ratios ($0.16 \pm 0.16 - 0.17 \pm 0.21$) between PE_North and PE_East, accompanied by only marginal increases in H/C. Their O/S ratios fell within a moderate range (2.39 ± 2.34 - 2.70 ± 2.83), with the proportion of $O/S \geq 4$ remaining essentially stable (16.7% - 21.9%). These characteristics suggested that CHOS+ species predominantly represented aromatic or heterocyclic sulfur-containing compounds, such as thiophenes and thioethers, which could be generated through high-temperature pyrolysis and cyclization processes. In contrast, CHOS- compounds displayed substantially lower DBE during PE_North (1.40 ± 2.38) and PE_East (1.78 ± 2.90) compared to MBGA (2.49 ± 3.10), alongside significant increases in O/C and OSc (Figure 4b and Table S3). Over 90% of CHOS- compounds exhibited $Xc < 2.5$ (Figure 4b, Figure S1, and Table S4), with O/S ratios rising from 2.12 ± 1.73 to 2.60 ± 1.89 and 2.74 ± 2.17. The proportion of CHOS- compounds with $O/S \geq 4$ increased from 25% to 40%, indicating their predominance as slightly unsaturated organic sulfides. This pattern suggested the substantial formation of organic sulfides (including alkyl sulfonates, carboxy sulfonic acids, and sulfate esters) during both pollution episodes. Higher O/C, OSc, and H/C values observed during PE_North were likely attributed to the formation of organosulfate in highly oxidized environments with enriched SO_2 and sulfate. Conversely, CHOS- compounds during PE_East may primarily be originated from gasoline vehicle exhaust, urban activities, and industrial sources.

Following the distribution of carbon oxidation state (Kroll et al., 2011), about 40% - 90% of detected molecules were classified into four types, and accounted for 35% - 90% of the bulk relative intensity. Hydrocarbon-like organic aerosol (HOA) and biomass burning organic aerosol (BBOA) are regarded as primary species directly emitted into the atmosphere, while semi-volatile and low-volatility oxidized organic aerosols (SV-OOA and LV-OOA) represent fresh and aged secondary aerosols formed

https://doi.org/10.5194/egusphere-2026-4499
Preprint. Discussion started: 1 September 2026

through multistep oxidation reactions (Jimenez et al., 2009; Kourtchev et al., 2015; Kourtchev et al., 2016). As demonstrated in Figure S3 and Table S5, both PE_North and PE_East periods exhibited higher proportions of BBOA or oxidized organic aerosol (including SV-OOA and LV-OOA) in terms of both formula number and relative intensity compared to MBGA, particularly for the increased fractions of LV-OOA and SV-OOA in CHO- and CHON- subgroups. This pattern aligned with the enhanced contributions of biomass burning emissions and aging processes during atmospheric transport. Similar classification by van Krevelen analysis (Figure S4, Table S6 and Table S7) (Kim et al., 2003; Fu et al., 2020) also suggested that the proportions of CRAMs-like structures (both ESI+ and ESI- modes) and aromatic structures (ESI+) within CHO, CHON, and CHOS subgroups increased progressively with pollution levels.

The relative intensity of CHN+ subgroups increased with pollution levels. These compounds exhibited N/C ratios primarily distributed between 0 – 0.3 (mean: 0.11 – 0.12) and H/C ratios of approximately 0.5 – 2.0 (mean: 1.04 – 1.19) (Figure S5a), and were detected across the *m/z* 100 – 600 range (Figure S5b), predominantly comprising N_1 and N_2 species. Both N/C and H/C values were comparatively low (Figure S5c), with 94.7% – 95.7% possessing $Xc \geq 2.5$ across all three periods. PAH-like components constituted 69.2% – 77.5% of CHN+ compounds (Figure S5c), substantially exceeding monocyclic aromatic hydrocarbons (17.7% – 25.5%), while aliphatic compounds represented only approximately 5% of the CHN+ subgroup.

https://doi.org/10.5194/egusphere-2026-4499
Preprint. Discussion started: 1 September 2026

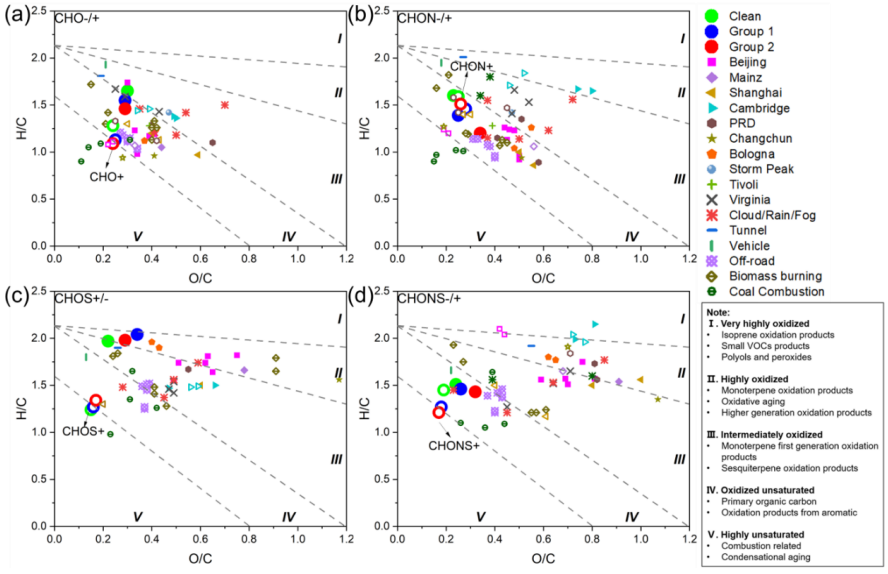

Figure 5. Comparison of O/C versus H/C ratios with previous studies, hollow and solid symbols present molecules detected in ESI+ and ESI- mode, respectively. The region marked in (a) CHO-/+, (b) CHON-/+, (c) CHOS-/+, and (d) CHONS-/+ were obtained from Zhang et al. (2021) to describe oxidation state of these compounds. (Reference: Beijing (Wang et al., 2018b; Jiang et al., 2016), Mainz (Wang et al., 2018b), Shanghai (Wang et al., 2021; Wang et al., 2017), Cambridge (Rincón et al., 2012), Peal River Delta (PRD, (Lin et al., 2012)), Guangzhou and Changchun (Wang et al., 2021), Po Vally in Bologna (Brege et al., 2018), Strom Peak Laboratory/mountain (Mazzoleni et al., 2012), Tivoli Industrial Estate and Docks (Kourtchev et al., 2014), Virginia (Willoughby et al., 2014), cloud-water (Bianco et al., 2018; Zhao et al., 2013), fog-water (Brege et al., 2018), urban rainwater (Altieri et al., 2009), tunnel OA (Tang et al., 2020), vehicle exhaust (Tang et al., 2020), off-road engine (Cui et al., 2019), biomass burning OA (Tang et al., 2020; Cai et al., 2020; Song et al., 2018), coal combustion OA (Tang et al., 2020; Song et al., 2018; Song et al., 2019)).

To compare the chemical characteristics of organic molecules detected over the ECS with previous studies, a modified van Krevelen diagram (Figure 5) based on the

https://doi.org/10.5194/egusphere-2026-4499
Preprint. Discussion started: 1 September 2026

maximum carbonyl ratio (Zhang et al., 2021) was constructed, dividing the diagram into five categories, i.e., very highly oxidized components, highly oxidized components, intermediately oxidized components, oxidized unsaturated components and highly unsaturated components. Both CHO+ and CHO- subgroups exhibited a shift towards higher unsaturation during PE_North and PE_East. Specifically, CHO+ molecules transitioned from region (IV) to region (V), suggesting a shift from primary source dominance towards combustion-related/condensational aging processes. CHO- molecules shifted from region (III) to region (IV), indicating increasing contributions from primary emissions and possible aromatic oxidation products. CHON+/- subgroups remained predominantly clustered within region (IV), though their distribution trended towards the lower right, signifying growing contributions from aromatic oxidation products originating from combustion-related/condensational aging precursors. The distributions of CHO+/- and CHON+/- subgroups overlapped with characteristic urban and emission source signatures, reflecting the combined influence of multiple emission sources and continental atmospheric transport on CHO and CHON molecules. CHOS+ subgroups distributed near the boundary between regions (IV) and (V), while CHOS- subgroups occupied region (II) with a rightward shift, aligning with distinct sources and formation pathways, as discussed in Section 3.3. CHONS+/- subgroups were primarily located in region (IV), with CHONS+ shifting towards region (V) and CHONS- towards region (III), indicating stronger combustion influence on CHONS+ and greater susceptibility to oxidation processes for CHONS-. Notably, the distributions of CHOS+/- and CHONS+/- subgroups showed less alignment with characteristic urban and emission source signatures compared to CHO+/- and CHON+/- subgroups, suggesting potential alternative sources or formation pathways for these molecular classes.

3.4 Differences of Organic Aerosol at the Molecular Level

3.4.1 Molecular Composition Dynamics Across Pollution Episodes

https://doi.org/10.5194/egusphere-2026-4499
Preprint. Discussion started: 1 September 2026

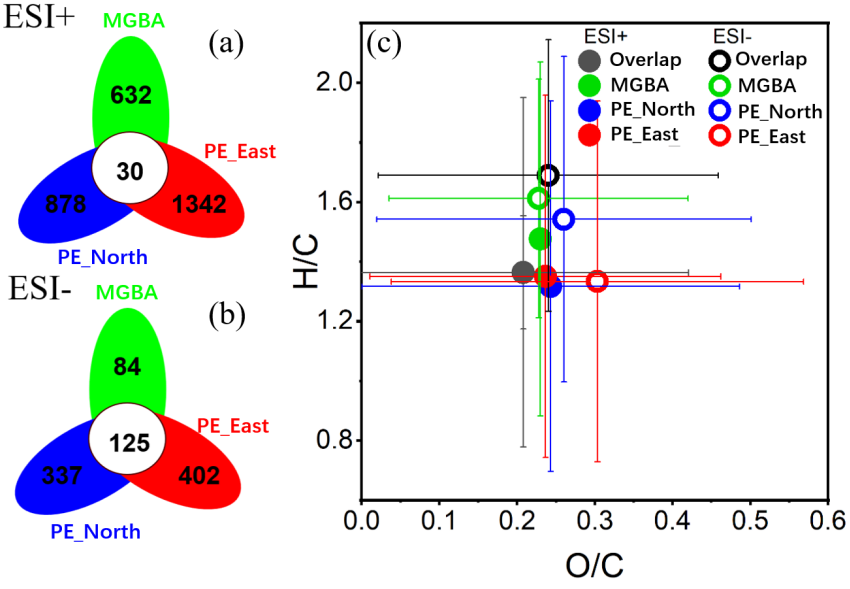

Figure 6. Wayne diagram of detected molecules during the three periods in the (a) ESI+ and (b) ESI- mode, and (c) O/C versus H/C of overlap and unique molecules during the three periods.

In the ESI+ mode, only 30 organic molecules were consistently detected during all three periods (Figure 6a), representing a mere 4.5%, 3.3%, and 2.2% of the total detected molecules, while 125 in the ESI- mode exhibited overlapping organic molecules, accounting for 40.2%, 27.1%, and 23.7% of molecules in each respective period (Figure 6b). This contrast underscored the strong temporal heterogeneity of organic aerosols over the East China Sea, resulting from distinct emission sources, chemical pathways, and meteorological conditions. Overlapping components in the ESI+ mode exhibited the lowest O/C ratios and moderate H/C values (Figure 6c), while those in the ESI- mode showed moderate O/C ratios but the highest H/C values. Unique components in both ionization modes during pollution episodes displayed higher O/C but substantially lower H/C compared to MBGA. Elevated O/C ratios suggested enriched oxygenated functional groups due to the secondary organic aerosol formation. Lower H/C ratios during pollution episodes resulted from aromatic structures from

https://doi.org/10.5194/egusphere-2026-4499
Preprint. Discussion started: 1 September 2026

522 combustion emissions, and the formation of highly functionalized stable compounds or
523 low-volatility oligomeric/polymeric products. Furthermore, unique components in the
524 ESI- mode during PE_East exhibited significantly higher O/C and lower H/C ratios
525 than during PE_North. This suggested unique components during PE_North may derive
526 more from aliphatic precursor dominated sources or undergo weak oxidation producing
527 aliphatic oxidation products, whereas unique components during PE_East likely
528 originated from aromatic-precursor-dominated sources and experienced strong
529 oxidation processes, such as aromatic ring-opening and nitro-substitution.
530

531 **3.4.2 Impact of Continental Outflow on Organic Aerosols at the Molecular Level**
532

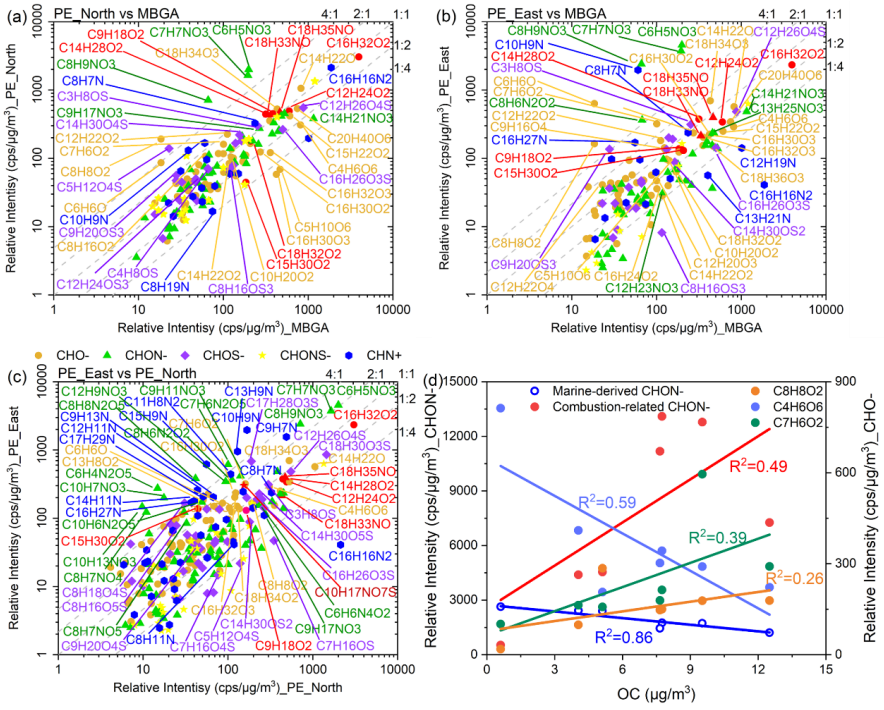

533

534 Figure 7. Comparison of the relative enrichment of identified compounds (CHO-,
535 CHON-, CHOS- CHONS- and CHN+) between (a) MBGA and PE_North, (b) MBGA
536 and PE_East, (c) PE_North and PE_East. All compounds are normalized to sampling
537 volume. (d) Correlations between OC and detected representative organic molecules in

https://doi.org/10.5194/egusphere-2026-4499
Preprint. Discussion started: 1 September 2026

CHO- and CHON- subgroups.

Figures 7a-7c depict the relative intensities of organic components (CHO-, CHON-, CHOS-, CHONS-, and CHN+) during the three periods. Palmitic acid ($C_{16}H_{32}O_2$), a key tracer for marine emissions (Filimonova et al., 2016; Sharmin et al., 2016), consistently exhibited the highest abundance among CHO- molecules during all periods. Its relative intensity remained comparable across periods, clustering near the 1:1 ratio line in inter-period comparisons. Notably, palmitic acid showed slightly higher relative abundance during PE_North, which could be due to the long-range transport over the ocean compared to the other two periods. Additionally, other characteristic tracers of marine biogenic emissions or oxidation products, including $C_{18}H_{33}NO$, $C_{18}H_{35}NO$, $C_9H_{18}O_2$ (azelaic acid), $C_{15}H_{30}O_2$, and $C_{18}H_{34}O_2$ (oleic acid), though less abundant than palmitic acid (Sharmin et al., 2016; Pavuluri et al., 2015; Hera, 2019), also displayed similar relative intensities across the three periods. This pattern further confirmed the stable contribution of marine biogenic emissions to atmospheric aerosols over the East China Sea.

Compared to MBGA (Figures 7a&7b), the highest-abundance CHO- species showed minimal variation across periods, dominated by long-chain aliphatic compounds with low unsaturation. However, increased relative abundance was observed for certain species from anthropogenic emissions and secondary formation. Biomass burning markers including C_6H_6O (phenol), $C_7H_6O_2$ (benzoic acid), and $C_8H_8O_2$ (methyl benzoate) (Hatch et al., 2015) exceeded the 2:1 line and approached the 4:1 line during PE_North and PE_East, respectively. CHON- compounds displayed significantly elevated nitro-aromatics (e.g., $C_6H_5NO_3$, $C_7H_7NO_3$, $C_8H_9NO_3$) above the 4:1 line during the two pollution episodes, these CHON- compounds were recognized as monocyclic aromatic structures originating from biomass burning (Mohr et al., 2013), fossil fuel combustion and secondary formation (Ng et al., 2017), which was evident from continental outflows. The relative intensities of CHOS- remained relatively stable for high-abundance species. Long-chain alkane CHOS- components ($C \geq 10$, e.g.,

https://doi.org/10.5194/egusphere-2026-4499
Preprint. Discussion started: 1 September 2026

$C_{12}H_{26}O_4S$, $C_{16}H_{26}O_3S$, $C_{14}H_{30}OS_2$) clustered between 2:1 – 1:2 lines with low unsaturation, reflecting mixed marine biogenic, fossil fuel combustion, and industrial sources. Besides, part of C ≥ 14 CHOS- compounds (e.g., $C_{18}H_{30}O_3S$, $C_{17}H_{28}O_3S$) showed pronounced increases above 2:1 and 4:1 lines, potentially linked to continental fossil fuel combustion and traffic emissions (Tang et al., 2020; Wang et al., 2016). Short-chain CHOS- components (C < 10, e.g., C_3H_8OS and $C_5H_{12}O_4S$) exhibited marked abundance enhancements above the 2:1 line during pollution episodes, which could be contributed by the secondary formation from transported unsaturated hydrocarbons (Tao et al., 2014). Likewise, CHN+ compounds demonstrated substantial increases in relative abundance during the two pollution episodes. Combustion-derived species such as C_9H_7N (quinoline, biomass burning (Schmeltz and Hoffmann, 1977)) and $C_{10}H_9N$ (naphthylamine, metal smelting and biomass burning (Ge et al., 2011)) both exceeded the 4:1 line.

The comparison between PE_East and PE_North revealed that aliphatic compounds behaved largely unchanged or slightly reduced under the PE_East air masses (Figure 7c). For instance, palmitic and azelaic acids showed marginally lower abundances during PE_East, falling below the 1:1 ratio line. This pattern likely reflects reduced marine biogenic contributions associated with weaker oceanic transport when air masses from the Yangtze River Delta region, though overall differences remained minor (proximity to 1:1 line). In contrast, PE_East exhibited elevated relative abundance of nitroaromatic compounds (Figure 7c), which can be attributed to enhanced NOx and nitrate concentrations under stronger photochemical oxidation conditions, promoting the secondary formation of nitroaromatics.

$C_4H_6O_6$, tentatively identified as tartaric acid, can be formed by oxidation of biogenic volatile organic compounds derived from marine biota (Röhrl and Lammel, 2002; Debolt et al., 2006). Tartaric acid and marine-derived CHON- species (long-chain compounds with O/N ≤ 2 associated with biogenic emissions) demonstrated strong inverse correlations with organic carbon ($R^2 = 0.59$ and $R^2 = 0.86$, respectively, Figure 7d). In contrast, $C_7H_6O_2$ and $C_8H_8O_2$, tentatively assigned as benzoic acid and

https://doi.org/10.5194/egusphere-2026-4499
Preprint. Discussion started: 1 September 2026

phenylacetic acid (representative combustion-derived phenolic compounds), exhibited positive correlations with OC concentrations (R^2 = 0.26 and R^2 = 0.39, respectively, Figure 7d). In parallel, combustion and secondary formation related CHON- species, including $C_6H_5NO_3$, $C_7H_7NO_3$, $C_8H_6N_2O_2$, and $C_8H_9NO_3$, exhibited strong positive correlations with OC (R^2 = 0.49) as well. The contrasting temporal trends of marine- and combustion-derived molecular tracers further revealed a shift in the secondary formation pathways of marine organic aerosols under continental outflow conditions. This transition was likely driven by the enhanced transport of anthropogenic precursors and elevated NOx levels associated with continental air masses. Such conditions favored the formation of anthropogenic secondary organic compounds, particularly nitrogen-containing oxidation products, while reducing the relative importance of secondary organic aerosol formation from marine biogenic precursors.

3.5 Evolution of Volatility Driven by Continental Outflows

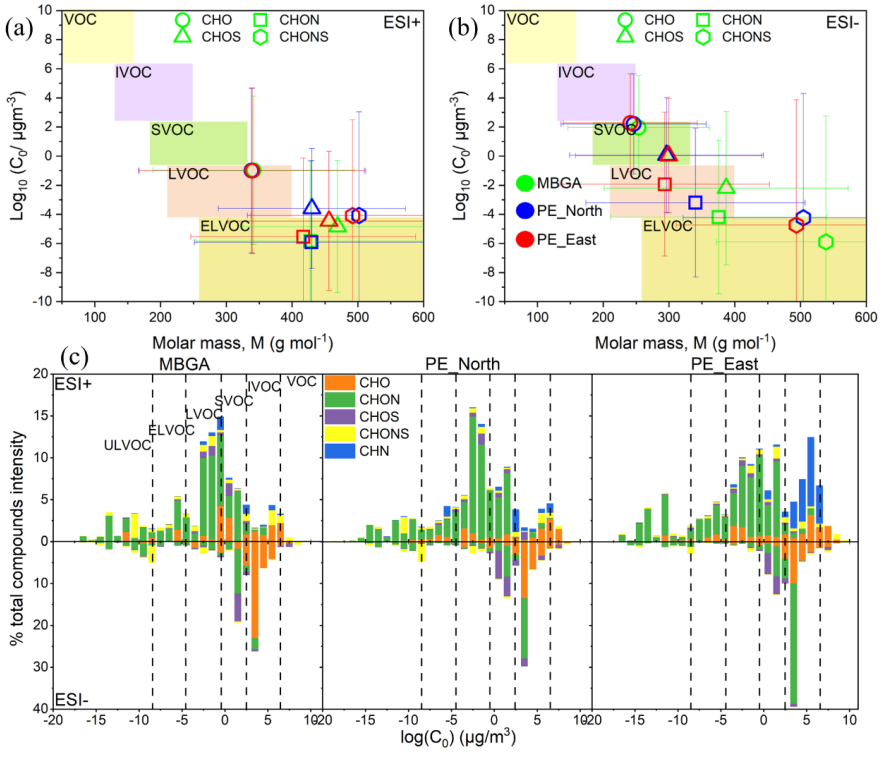

https://doi.org/10.5194/egusphere-2026-4499
Preprint. Discussion started: 1 September 2026

Figure 8. Mean molar mass versus saturation mass concentration for organic compounds categorized by CHO, CHON, CHOS and CHONS in the (a) ESI+ and (b) ESI- mode, (c) relative contribution of organic compounds with different volatility.

The volatility of organic molecule is a critical property governing vapor condensation, gas-particle partitioning, new particle formation, and particulate growth, which is closely linked to functional groups and oxidation state. Figures 8a&8b illustrate the relationship between saturation concentration and molar mass for all detected subgroups. The CHO+ and CHO- subgroups predominantly fell within the LVOC and SVOC volatility ranges, respectively, showing similar distributions across periods. As shown in Figure S6 and Table S8, IVOC species constituted the highest proportion (30 – 35%) of CHO+ compounds, while LVOC species, SVOC species, and ELVOC species contributions were comparable (~20 – 25% each). CHO- compounds were dominated by IVOC species (~50%), followed by SVOC species (33 – 40%), with minimal LVOC/ELVOC species representation (<9%). Similarly, CHON+, CHOS+, and CHONS+/- subgroups predominantly clustered near the LVOC-ELVOC boundary despite minor variations. CHON+ compounds showed high ELVOC species prevalence (~50%), followed by LVOC species and SVOC species, indicating overall low volatility. CHOS+ displayed comparable ELVOC species and LVOC species contributions (~40%) with lower SVOC species proportions (14 – 18%). Both CHONS+ and CHONS- subgroups followed identical volatility hierarchies of ELVOC species > LVOC species > SVOC species > IVOC species.

Conversely, CHON-, CHOS-, and CHN+ subgroups exhibited substantial variations in molecular volatility and relative abundance contributions across periods. Specifically, CHON- during MBGA clustered near the LVOC-ELVOC boundary. With increasing pollution intensity and rising NO_2/nitrate levels, its distribution shifted towards higher volatility (ELVOC→LVOC→SVOC). Meanwhile, both molecular number and relative intensity of ELVOC species in CHON- decreased significantly, while SVOC contributions surged from 4.33% (MBGA) to 30.0% and 39.9% (Figure

https://doi.org/10.5194/egusphere-2026-4499
Preprint. Discussion started: 1 September 2026

S6 and Table S8). CHOS- shifted from the LVOC region (MBGA) to the SVOC-IVOC transition zone during both pollution episodes.

As shown in Figure 8c, among volatility bins ($log_{10}C_0$ = 1), CHON- during two pollution episodes showed the most pronounced increase within the IVOC range compared to MBGA. Contrastingly, SVOC species consistently dominated CHOS- subgroup (65–70%), and maintained stable relative intensity contributions, with molecular proportion increased from 30.7% → 53.4% during the episode from MBGA to pollution episodes, while the relative intensity of ELVOC species decreased from 28.2% to 11.9% (Figure S6, Table S8). CHN+ volatility differences manifested as LVOC species dominance (~50%) during MBGA, balanced distributions with prominent SVOC species contribution (~40%) in PE_North, and PE_East dominance by IVOC species (>50% molecular proportion, >80% relative abundance). Figure 8c further highlights the exceptional increase in total organic aerosol relative intensity contributed by IVOC-range CHN+ molecules.

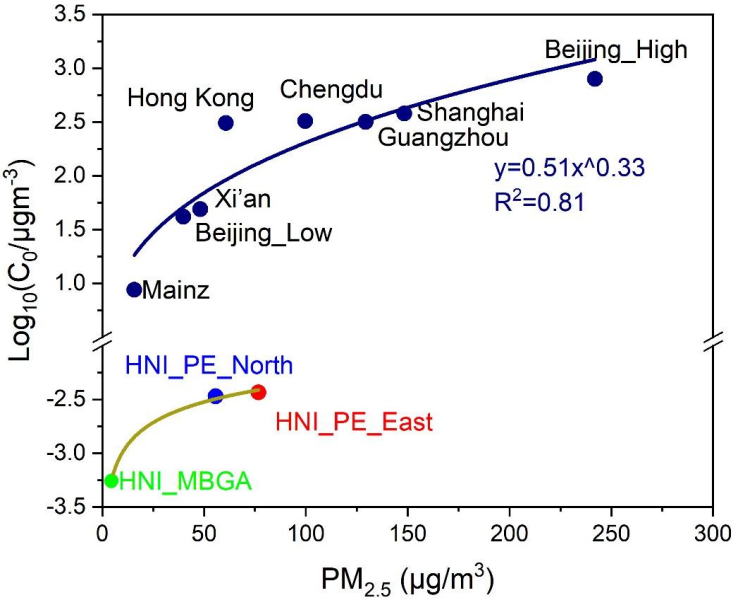

Figure 9. Scatter plots of distribution of $PM_{2.5}$ mass concentration versus mean volatility. Other city data are obtained from Figure S12 and Table S3 in Wang et al. (2024), and a

https://doi.org/10.5194/egusphere-2026-4499
Preprint. Discussion started: 1 September 2026

summary table is given in Table S9.

Wang et al. (2024) established a logarithmic correlation between $PM_{2.5}$ concentrations and bulk organic aerosol OA volatility across urban areas (Figure 9), indicating enhanced volatility with worsening urban air pollution. Despite methodological differences in solvent extraction affecting absolute volatility magnitudes, a similar relationship emerged between $PM_{2.5}$ levels and average OA volatility in the East China Sea. This trend likely reflected increased contributions from less-oxidized primary OA during pollution episodes (Xu et al., 2021). Elevated particle number concentrations from anthropogenic and primary OA emissions provided greater surface area for organic vapor condensation onto particles, thereby suppressing gas-phase oxidation. Xu et al. (2021) documented higher wintertime OA volatility in rural and urban North China Plain due to enhanced coal and biomass burning emissions. Negligible volatility changes in CHO+/-, CHON+, CHOS+, and CHONS+/- subgroups were attributable to dominant contributions from transported higher-volatility primary emissions outweighing oxidation effects, a pattern particularly pronounced in the CHN+ subgroup. In particular, the CHON− and CHOS− subgroups exhibited significantly higher volatility during PE_North and PE_East, likely reflecting enhanced contributions from semi-volatile organic nitrates and organosulfates formed under elevated NOx and SO_2 conditions.

To elucidate the volatility transformation of organic aerosols across the three periods, individual compound distributions within the molecular corridors framework are presented in Figure S7 (Li et al., 2016; Shiraiwa et al., 2014).The molecular corridor is constrained by two boundary layer of alkanes (C_nH_{2n+2}, grey line with O/C=0) and sugar alcohols ($C_nH_{2n+2}O_n$, yellow line with O/C=1). In this study, organic molecules over the East China Sea exhibited decreasing volatility with increasing molecular weight, consistent with urban OA studies (Li et al., 2016; Wang et al., 2024). CHO+/-, CHON+, CHOS+, and CHONS+/- subgroups showed intermingled distributions across periods, whereas CHON- and CHOS- molecules shifted towards the upper SVOC-

https://doi.org/10.5194/egusphere-2026-4499
Preprint. Discussion started: 1 September 2026

IVOC corridor region during PE_North and PE_East. This migration suggested such CHON- and CHOS- components were formed via gas-phase or aqueous-phase oxidation of smaller molecular-weight VOC precursors (Shiraiwa et al., 2014). Figure S8 further illustrates the relationship between volatility and OSc. Compounds in the ESI+ mode concentrated within $-2 < OSc < 0$, indicating low oxidation states with broad volatility distributions (Figure S8a). The volatile species with high relative intensity were characterized of relatively low OSc and O/C values, while some high-OSc compounds exhibited minimal volatility. In contrast, compounds in the ESI- mode (Figure S8b) displayed an exponential volatility-OSc relationship. Elevated OSc corresponded to higher volatility coupled with greater relative intensity, particularly for $CHON^-$ and $CHOS^-$ subgroups, which aligned with our preceding discussion.

4. Conclusion

Significant uncertainties persist in accurately assessing the climate effects of ambient organic aerosol due to its complex molecular composition and diverse sources. In this study, the profound influence of East Asian continental outflows on the molecular characteristics of organic aerosol over the East China Sea was investigated. During MBGA, the mass concentration of $PM_{2.5}$ was only 4.4 $\mu g/m^3$, while it reached 55.7 $\mu g/m^3$ and 76.7 $\mu g/m^3$ during two polluted periods, i.e., PE_North and PE_East, respectively. Air masses during PE_North originated from northern China and travelled over marine areas, resulting in higher relative humidity. Air masses during PE_East originated from the Yangtze River Delta region, accompanied with higher downward solar radiation and O_3 concentrations.

A total of 569 – 829 and 278 – 383 organic compounds were detected in ESI+ and ESI- modes, respectively, which exhibited relatively low O/C ratios (0 – 0.6) but broad H/C distributions (< 2.5). In the ESI+ mode, CHON+ compounds dominated (55 – 58% relative intensity). CHO- species prevailed in the ESI- mode (41.0% during MBGA), with CHON- as the second-most abundant subgroup (~35%). Only 4.5% (ESI+) and 23.7 – 40.2% (ESI-) of the organic compounds were detected across all periods,

https://doi.org/10.5194/egusphere-2026-4499
Preprint. Discussion started: 1 September 2026

indicating extreme sensitivity of molecular compositions to continental outflows. Unique compounds during pollution episodes exhibited elevated O/C and reduced H/C, consistent with molecular characteristics from combustion sources and oxidative functionalization. Pollution episodes significantly enriched combustion tracers with high unsaturation (DBE $\geq$ 4) and aromaticity (Xc $\geq$ 2.50) compared to MBGA. CHON- abundance progressively rose to 36.2% (PE_North) and 51.7% (PE_East), while CHNS*+ increased to 16.8% (PE_East). CHON- compounds showed substantial oxidation enhancement, with mean O/C increasing from 0.23 ± 0.20 to 0.34 ± 0.22. The proportion of nitroaromatics (O/N $\geq$ 3) surged from 24.7% to 46.7%, confirming dominance by biomass burning and coal combustion emissions or their nitro-precursors. Similarly, characteristic combustion products like quinoline (C_9H_7N) and naphthylamine ($C_{10}H_9N$) exhibited 4-fold increases during pollution episodes, directly reflecting contributions from fossil fuel combustion and industrial emissions.

Long-chain fatty acids (e.g., palmitic acid and oleic acid) dominated CHO- compositions during MBGA. Their abundances increased during PE_North due to extended trajectories of marine air masses, while only marginal decreases occurred during PE_East, demonstrating pronounced resilience of marine biogenic contributions. Meanwhile, short-chain CHOS- species doubled through secondary formation from alkenes, while monoterpene oxidation products (e.g., $C_{10}H_{17}NO_7S$) only emerged exclusively during pollution episodes, suggesting the addition of anthropogenic secondary formation in the marine atmosphere. Under the high-humidity and sulfate-rich conditions during PE_North, aqueous-phase oxidation promoted the formation of organosulfate (O/S $\geq$ 4 in CHOS-) and SV-OOA, concurrently driving CHOS- volatility shift towards the SVOC regime under acidic conditions (Zhu et al., 2024). Conversely, high irradiation and NOx under PE_East generated highly oxidized nitroaromatics, though excess NOx limited VOC conversion to lower-volatility products and triggered IVOC predominance in CHON-. This volatility dichotomy underscored pathway-specific secondary processing mechanisms. Furthermore, bulk OA volatility increased

https://doi.org/10.5194/egusphere-2026-4499
Preprint. Discussion started: 1 September 2026

logarithmically with $PM_{2.5}$ concentrations during pollution episodes, primarily attributable to enhanced contributions from higher-volatility primary emissions.

In summary, East Asian continental outflows profoundly reshaped the molecular compositions and evolution pathways of organic aerosols over the East China Sea. This influence superseded marine emissions, induced various oxidative processes, and caused molecular evolution of organic aerosol microphysics. Our findings provide critical constraints for climate models, with profound implications for regional climate predictability and emission control strategies.

Author contribution

H.L. and K. H. designed this study. H.L. performed measurements and data analysis. X.Q., Q.G., and X.W. performed data collection. All have commented and reviewed the paper.

Competing interests

The authors declare that they have no conflict of interest.

Data availability

All datasets used in this study are publicly available on Figshare (https://doi.org/10.6084/m9.figshare.33103328) (Li et al., 2026).

Acknowledgment

This work was financially supported by the National Natural Science Foundation of China (42505096, 42575107, 42275105, 42361144711), and the National Key R&D Plan Programs (2018YFC0213105). We extend our deepest gratitude to the residents of Huaniao Island, particularly Mr. Yueping Chen and Mrs. Yaping Zhang, for their invaluable support of our atmosphere and marine observation program since 2014, and for their generous hospitality toward our research team members.

https://doi.org/10.5194/egusphere-2026-4499
Preprint. Discussion started: 1 September 2026

References:

Ajith, T. C., Kompalli, S. K., Nair, V. S., Gogoi, M., Jayachandran, V., and Babu, S. S.: Evolution of Organic Aerosols in the South Asian Outflow to the Northern Indian Ocean, ACS Earth and Space Chemistry, 7, 2190-2204, 10.1021/acsearthspacechem.3c00059, 2023.

Albert, M. F. M. A., Schaap, M., de Leeuw, G., and Builtjes, P. J. H.: Progress in the determination of the sea spray source function using satellite data, J Integr Environ Sci, 7, 159-166, 10.1080/19438151003621466, 2010.

Allen H. Goldstein and Galbally, I. E.: Known and Unexplored Organic Constituents in the Earth's Atmosphere, Environmental Science & Technology, 41, 1514-1521, 10.1021/es072476p, 2007.

Altieri, K. E., Turpin, B. J., and Seitzinger, S. P.: Oligomers, organosulfates, and nitrooxy organosulfates in rainwater identified by ultra-high resolution electrospray ionization FT-ICR mass spectrometry, Atmospheric Chemistry and Physics, 9, 2533-2542, DOI 10.5194/acp-9-2533-2009, 2009.

Bao, H., Niggemann, J., Luo, L., Dittmar, T., and Kao, S.-J.: Molecular composition and origin of water-soluble organic matter in marine aerosols in the Pacific off China, Atmospheric Environment, 191, 27-35, https://doi.org/10.1016/j.atmosenv.2018.07.059, 2018.

Bianco, A., Deguillaume, L., Vaïtilingom, M., Nicol, E., Baray, J.-L., Chaumerliac, N., and Bridoux, M.: Molecular Characterization of Cloud Water Samples Collected at the Puy de Dôme (France) by Fourier Transform Ion Cyclotron Resonance Mass Spectrometry, Environmental Science & Technology, 52, 10275-10285, 10.1021/acs.est.8b01964, 2018.

Bikkina, P., Bikkina, S., Kawamura, K., Sarma, V. V. S. S., and Deshmukh, D. K.: Unraveling the sources of atmospheric organic aerosols over the Arabian Sea: Insights from the stable carbon and nitrogen isotopic composition, Sci Total Environ, 827, 154260, https://doi.org/10.1016/j.scitotenv.2022.154260, 2022.

Brege, M., Paglione, M., Gilardoni, S., Decesari, S., Facchini, M. C., and Mazzoleni, L. R.: Molecular insights on aging and aqueous-phase processing from ambient biomass burning emissions-influenced Po Valley fog and aerosol, Atmospheric Chemistry and Physics, 18, 13197-13214, 10.5194/acp-18-13197-2018, 2018.

Brüggemann, M., Hayeck, N., and George, C.: Interfacial photochemistry at the ocean surface is a global source of organic vapors and aerosols, Nature Communications, 9, ARTN 2101 10.1038/s41467-018-04528-7, 2018.

Burrows, S. M., Easter, R. C., Liu, X., Ma, P. L., Wang, H., Elliott, S. M., Singh, B., Zhang, K., and Rasch, P. J.: OCEANFILMS (Organic Compounds from Ecosystems to Aerosols: Natural Films and Interfaces via Langmuir Molecular Surfactants) sea spray organic aerosol emissions – implementation in a global climate model and impacts on clouds, Atmos. Chem. Phys., 22, 5223-5251, 10.5194/acp-22-5223-2022, 2022.

Cai, J., Zeng, X. Y., Zhi, G. R., Gligorovski, S., Sheng, G. Y., Yu, Z. Q., Wang, X. M., and Peng, P. A.: Molecular composition and photochemical evolution of water-soluble organic carbon (WSOC) extracted from field biomass burning aerosols using high-resolution mass spectrometry, Atmospheric Chemistry and Physics, 20, 6115-6128, 10.5194/acp-20-6115-2020, 2020.

Claeys, M., Wang, W., Vermeylen, R., Kourtchev, I., Chi, X., Farhat, Y., Surratt, J. D., Gómez-González, Y., Sciare, J., and Maenhaut, W.: Chemical characterisation of marine aerosol at Amsterdam Island during the austral summer of 2006–2007, Journal of Aerosol Science, 41, 13-22, https://doi.org/10.1016/j.jaerosci.2009.08.003, 2010.

Cochran, R. E., Laskina, O., Trueblood, J. V., Estillore, A. D., Morris, H. S., Jayarathne, T., Sultana, C.

https://doi.org/10.5194/egusphere-2026-4499
Preprint. Discussion started: 1 September 2026

M., Lee, C., Lin, P., Laskin, J., Laskin, A., Dowling, J. A., Qin, Z., Cappa, C. D., Bertram, T. H., Tivanski, A. V., Stone, E. A., Prather, K. A., and Grassian, V. H.: Molecular Diversity of Sea Spray Aerosol Particles: Impact of Ocean Biology on Particle Composition and Hygroscopicity, Chem, 2, 655-667, 10.1016/j.chempr.2017.03.007, 2017.

Cui, M., Li, C., Chen, Y. J., Zhang, F., Li, J., Jiang, B., Mo, Y. Z., Li, J., Yan, C. Q., Zheng, M., Xie, Z. Y., Zhang, G., and Zheng, J. Y.: Molecular characterization of polar organic aerosol constituents in off-road engine emissions using Fourier transform ion cyclotron resonance mass spectrometry (FT-ICR MS): implications for source apportionment, Atmospheric Chemistry and Physics, 19, 13945-13956, 10.5194/acp-19-13945-2019, 2019.

DeBolt, S., Cook, D. R., and Ford, C. M.: L-Tartaric acid synthesis from vitamin C in higher plants, Proceedings of the National Academy of Sciences, 103, 5608-5613, 2006.

Donahue, N. M., Epstein, S. A., Pandis, S. N., and Robinson, A. L.: A two-dimensional volatility basis set: 1. organic-aerosol mixing thermodynamics, Atmos. Chem. Phys., 11, 3303-3318, 10.5194/acp-11-3303-2011, 2011.

Dong, J., Li, F., and Xie, K.: Study on the source of polycyclic aromatic hydrocarbons (PAHs) during coal pyrolysis by PY–GC–MS, Journal of Hazardous Materials, 243, 80-85, https://doi.org/10.1016/j.jhazmat.2012.09.073, 2012.

Erickson, D. J. and Duce, R. A.: On the Global Flux of Atmospheric Sea Salt, Journal of Geophysical Research-Oceans, 93, 14079-14088, DOI 10.1029/JC093iC11p14079, 1988.

Filimonova, V., Gonçalves, F., Marques, J. C., De Troch, M., and Gonçalves, A. M. M.: Fatty acid profiling as bioindicator of chemical stress in marine organisms: A review, Ecological Indicators, 67, 657-672, https://doi.org/10.1016/j.ecolind.2016.03.044, 2016.

Franklin, E. B., Yee, L. D., Wernis, R., Isaacman-VanWertz, G., Kreisberg, N., Weber, R., Zhang, H., Palm, B. B., Hu, W., Campuzano-Jost, P., Day, D. A., Manzi, A., Artaxo, P., Souza, R. A. F. D., Jimenez, J. L., Martin, S. T., and Goldstein, A. H.: Chemical Signatures of Seasonally Unique Anthropogenic Influences on Organic Aerosol Composition in the Central Amazon, Environmental Science & Technology, 57, 6263-6272, 10.1021/acs.est.2c07260, 2023.

Frossard, A. A., Russell, L. M., Burrows, S. M., Elliott, S. M., Bates, T. S., and Quinn, P. K.: Sources and composition of submicron organic mass in marine aerosol particles, J Geophys Res-Atmos, 119, 12977-13003, 2014.

Fu, P. Q., Kawamura, K., Chen, J., Charriere, B., and Sempere, R.: Organic molecular composition of marine aerosols over the Arctic Ocean in summer: contributions of primary emission and secondary aerosol formation, Biogeosciences, 10, 653-667, 10.5194/bg-10-653-2013, 2013.

Fu, Q.-L., Fujii, M., and Riedel, T.: Development and comparison of formula assignment algorithms for ultrahigh-resolution mass spectra of natural organic matter, Analytica Chimica Acta, 1125, 247-257, https://doi.org/10.1016/j.aca.2020.05.048, 2020.

Gantt, B. and Meskhidze, N.: The physical and chemical characteristics of marine primary organic aerosol: a review, Atmos. Chem. Phys., 13, 3979-3996, 10.5194/acp-13-3979-2013, 2013.

Ge, B., Xu, X., Ma, Z., Pan, X., Wang, Z., Lin, W., Ouyang, B., Xu, D., Lee, J., Zheng, M., Ji, D., Sun, Y., Dong, H., Squires, F. A., Fu, P., and Wang, Z.: Role of Ammonia on the Feedback Between AWC and Inorganic Aerosol Formation During Heavy Pollution in the North China Plain, 6, 1675-1693, https://doi.org/10.1029/2019EA000799, 2019.

Ge, X., Wexler, A. S., and Clegg, S. L.: Atmospheric amines – Part I. A review, Atmospheric Environment, 45, 524-546, https://doi.org/10.1016/j.atmosenv.2010.10.012, 2011.

https://doi.org/10.5194/egusphere-2026-4499
Preprint. Discussion started: 1 September 2026

Guo, H., Liu, J., Froyd, K. D., Roberts, J. M., Veres, P. R., Hayes, P. L., Jimenez, J. L., Nenes, A., and Weber, R. J.: Fine particle pH and gas–particle phase partitioning of inorganic species in Pasadena, California, during the 2010 CalNex campaign, Atmos Chem Phys, 17, 5703-5719, 10.5194/acp-17-5703-2017, 2017.

Guo, Z., Wang, J., Chen, X., Cui, F., Wang, T., Zhou, C., Song, G., Zhang, S., and Chen, J.: Photochemistry of dissolved organic matter extracted from coastal seawater: Excited triplet-states and contents of phenolic moieties, Water Research, 188, 116568, https://doi.org/10.1016/j.watres.2020.116568, 2021.

Gurganus, S. C., Wozniak, A. S., and Hatcher, P. G.: Molecular characteristics of the water soluble organic matter in size-fractionated aerosols collected over the North Atlantic Ocean, Marine Chemistry, 170, 37-48, https://doi.org/10.1016/j.marchem.2015.01.007, 2015.

Hasenecz, E. S., Kaluarachchi, C. P., Lee, H. D., Tivanski, A. V., and Stone, E. A.: Saccharide Transfer to Sea Spray Aerosol Enhanced by Surface Activity, Calcium, and Protein Interactions, Acs Earth and Space Chemistry, 3, 2539-2548, 10.1021/acsearthspacechem.9b00197, 2019.

Hatch, L. E., Luo, W., Pankow, J. F., Yokelson, R. J., Stockwell, C. E., and Barsanti, K. C.: Identification and quantification of gaseous organic compounds emitted from biomass burning using two-dimensional gas chromatography–time-of-flight mass spectrometry, Atmos. Chem. Phys., 15, 1865-1899, 10.5194/acp-15-1865-2015, 2015.

Heaton, K. J., Sleighter, R. L., Hatcher, P. G., Hall, W. A. I. V., and Johnston, M. V.: Composition Domains in Monoterpene Secondary Organic Aerosol, Environmental Science & Technology, 43, 7797-7802, 10.1021/es901214p, 2009.

Hegde, P., Boreddy, S. K. R., Aswini, A. R., and Aryasree, S.: Influence of south Asian outflow on secondary organic aerosol formation over the Indian Ocean: Inferences from water-soluble low molecular weight dicarboxylic acids and related organic compounds during ICARB 2018 experiment, Marine Chemistry, 239, 104071, https://doi.org/10.1016/j.marchem.2021.104071, 2022.

Hera, A.: Chemical signaling in diatom-parasite interactions, Friedrich-Schiller-Universität Jena, 2019.

Jang, M., Lee, S., and Kamens, R. M.: Organic aerosol growth by acid-catalyzed heterogeneous reactions of octanal in a flow reactor, Atmospheric Environment, 37, 2125-2138, https://doi.org/10.1016/S1352-2310(03)00077-3, 2003.

Jayarathne, T., Sultana, C. M., Lee, C., Malfatti, F., Cox, J. L., Pendergraft, M. A., Moore, K. A., Azam, F., Tivanski, A. V., Cappa, C. D., Bertram, T. H., Grassian, V. H., Prather, K. A., and Stone, E. A.: Enrichment of Saccharides and Divalent Cations in Sea Spray Aerosol During Two Phytoplankton Blooms, Environmental Science & Technology, 50, 11511-11520, 10.1021/acs.est.6b02988, 2016.

Ji, X., Zhao, M.-L., Zhang, J., and Yang, G.-P.: Spatial variation in the optical and molecular properties of dissolved organic matter in the Yellow Sea and East China Sea, Progress in Oceanography, 220, 103192, https://doi.org/10.1016/j.pocean.2023.103192, 2024.

Jiang, B., Kuang, B. Y., Liang, Y. M., Zhang, J. Y., Huang, X. H. H., Xu, C. M., Yu, J. Z., and Shi, Q.: Molecular composition of urban organic aerosols on clear and hazy days in Beijing: a comparative study using FT-ICR MS, Environ Chem, 13, 888-901, 10.1071/En15230, 2016.

Jiang, X., Rotily, L., Villermaux, E., and Wang, X.: Submicron drops from flapping bursting bubbles, 119, e2112924119, 10.1073/pnas.2112924119 %J Proceedings of the National Academy of Sciences, 2022.

Jimenez, J. L., Canagaratna, M. R., Donahue, N. M., Prevot, A. S. H., Zhang, Q., Kroll, J. H., DeCarlo, P. F., Allan, J. D., Coe, H., Ng, N. L., Aiken, A. C., Docherty, K. S., Ulbrich, I. M., Grieshop, A. P.,

https://doi.org/10.5194/egusphere-2026-4499
Preprint. Discussion started: 1 September 2026

Robinson, A. L., Duplissy, J., Smith, J. D., Wilson, K. R., Lanz, V. A., Hueglin, C., Sun, Y. L., Tian, J., Laaksonen, A., Raatikainen, T., Rautiainen, J., Vaattovaara, P., Ehn, M., Kulmala, M., Tomlinson, J. M., Collins, D. R., Cubison, M. J., E., Dunlea, J., Huffman, J. A., Onasch, T. B., Alfarra, M. R., Williams, P. I., Bower, K., Kondo, Y., Schneider, J., Drewnick, F., Borrmann, S., Weimer, S., Demerjian, K., Salcedo, D., Cottrell, L., Griffin, R., Takami, A., Miyoshi, T., Hatakeyama, S., Shimono, A., Sun, J. Y., Zhang, Y. M., Dzepina, K., Kimmel, J. R., Sueper, D., Jayne, J. T., Herndon, S. C., Trimborn, A. M., Williams, L. R., Wood, E. C., Middlebrook, A. M., Kolb, C. E., Baltensperger, U., and Worsnop, D. R.: Evolution of Organic Aerosols in the Atmosphere, Science, 326, 1525-1529, doi:10.1126/science.1180353, 2009.

Jo, D. S., Nault, B. A., Tilmes, S., Gettelman, A., McCluskey, C. S., Hodzic, A., Henze, D. K., Nawaz, M. O., Fung, K. M., and Jimenez, J. L.: Global Health and Climate Effects of Organic Aerosols from Different Sources, Environmental Science & Technology, 57, 13793-13807, 10.1021/acs.est.3c02823, 2023.

Kang, M., Fu, P., Kawamura, K., Yang, F., Zhang, H., Zang, Z., Ren, H., Ren, L., Zhao, Y., Sun, Y., and Wang, Z.: Characterization of biogenic primary and secondary organic aerosols in the marine atmosphere over the East China Sea, Atmos. Chem. Phys., 18, 13947-13967, 10.5194/acp-18-13947-2018, 2018.

Kim, S., Kramer, R. W., and Hatcher, P. G.: Graphical Method for Analysis of Ultrahigh-Resolution Broadband Mass Spectra of Natural Organic Matter, the Van Krevelen Diagram, Analytical Chemistry, 75, 5336-5344, 10.1021/ac034415p, 2003.

Kiontke, A., Oliveira-Birkmeier, A., Opitz, A., and Birkemeyer, C.: Electrospray Ionization Efficiency Is Dependent on Different Molecular Descriptors with Respect to Solvent pH and Instrumental Configuration, PLOS ONE, 11, e0167502, 10.1371/journal.pone.0167502, 2016.

Kourtchev, I., Doussin, J. F., Giorio, C., Mahon, B., Wilson, E. M., Maurin, N., Pangui, E., Venables, D. S., Wenger, J. C., and Kalberer, M.: Molecular composition of fresh and aged secondary organic aerosol from a mixture of biogenic volatile compounds: a high-resolution mass spectrometry study, Atmos. Chem. Phys., 15, 5683-5695, 10.5194/acp-15-5683-2015, 2015.

Kourtchev, I., O'Connor, I. P., Giorio, C., Fuller, S. J., Kristensen, K., Maenhaut, W., Wenger, J. C., Sodeau, J. R., Glasius, M., and Kalberer, M.: Effects of anthropogenic emissions on the molecular composition of urban organic aerosols: An ultrahigh resolution mass spectrometry study, Atmospheric Environment, 89, 525-532, 10.1016/j.atmosenv.2014.02.051, 2014.

Kourtchev, I., Godoi, R. H. M., Connors, S., Levine, J. G., Archibald, A. T., Godoi, A. F. L., Paralovo, S. L., Barbosa, C. G. G., Souza, R. A. F., Manzi, A. O., Seco, R., Sjostedt, S., Park, J. H., Guenther, A., Kim, S., Smith, J., Martin, S. T., and Kalberer, M.: Molecular composition of organic aerosols in central Amazonia: an ultra-high-resolution mass spectrometry study, Atmos. Chem. Phys., 16, 11899-11913, 10.5194/acp-16-11899-2016, 2016.

Kroll, J. H., Donahue, N. M., Jimenez, J. L., Kessler, S. H., Canagaratna, M. R., Wilson, K. R., Altieri, K. E., Mazzoleni, L. R., Wozniak, A. S., and Bluhm, H. J. N. c.: Carbon oxidation state as a metric for describing the chemistry of atmospheric organic aerosol, 3, 133-139, 2011.

Lawler, M. J., Lewis, S. L., Russell, L. M., Quinn, P. K., Bates, T. S., Coffman, D. J., Upchurch, L. M., and Saltzman, E. S.: North Atlantic marine organic aerosol characterized by novel offline thermal desorption mass spectrometry: polysaccharides, recalcitrant material, and secondary organics, Atmos. Chem. Phys., 20, 16007-16022, 10.5194/acp-20-16007-2020, 2020.

Leaitch, W. R., Russell, L. M., Liu, J., Kolonjari, F., Toom, D., Huang, L., Sharma, S., Chivulescu, A., Veber, D., and Zhang, W. D.: Organic functional groups in the submicron aerosol at 82.5 degrees N, 62.5 degrees W from 2012 to 2014, Atmos Chem Phys, 18, 3269-3287, 10.5194/acp-18-3269-2018, 2018.

https://doi.org/10.5194/egusphere-2026-4499
Preprint. Discussion started: 1 September 2026

Li, H., Wang, L., Qin, X., Wang, G., Fu, M., Chen, C., Xu, J., Deng, C., and Huang, K.: Seasonal differences in continental outflows and marine emissions of organic aerosols in the East China Sea: Insight from the variation of saccharides, Atmospheric Research, 295, 107031, https://doi.org/10.1016/j.atmosres.2023.107031, 2023a.

Li, H., Qin, X., Wang, G., Xu, J., Wang, L., Lu, D., Liu, C., Zheng, H., Liu, J., Huang, K., and Deng, C.: Conjoint impacts of continental outflows and marine sources on brown carbon in the East China sea: Abundances, optical properties, and formation processes, Atmospheric Environment, 273, 118959, https://doi.org/10.1016/j.atmosenv.2022.118959, 2022a.

Li, H., Qin, X., Wang, G., Xu, J., Wang, L., Lu, D., Liu, C., Zheng, H., Liu, J., Huang, K., and Deng, C.: Conjoint impacts of continental outflows and marine sources on brown carbon in the East China sea: Abundances, optical properties, and formation processes, Atmos Environ, 273, 10.1016/j.atmosenv.2022.118959, 2022b.

Li, H., Qin, X., Chen, J., Wang, G., Liu, C., Lu, D., Zheng, H., Song, X., Gao, Q., Xu, J., Zhu, Y., Liu, J., Wang, X., Deng, C., and Huang, K.: Continuous Measurement and Molecular Compositions of Atmospheric Water-Soluble Brown Carbon in the Nearshore Marine Boundary Layer of Northern China: Secondary Formation and Influencing Factors, 128, e2023JD038565, https://doi.org/10.1029/2023JD038565, 2023b.

Li, H., Qin, X., Xu, J., Gao, Q., Bi, K., Deng, Z., Liu, J., Zheng, H., Ren, X., Wang, X., Deng, C., Huang, K.: Measurement Report: Molecular Dynamics of Organic Aerosol in the Wintertime East China Sea Driven by East Asian Outflows, Figshare [dataset], https://doi.org/10.6084/m9.figshare.33103328, 2026.

Li, S., Wang, Y., Zhang, Y., Yi, Y., Wang, Y., Guo, Y., Yu, C., Jiang, Y., Shi, J., Zhang, C., Zhu, J., Hu, W., Yu, J., Yao, X., Gao, H., and Hu, M.: Atmospheric organosulfate formation regulated by continental outflows and marine emissions over East Asian marginal seas, Atmos. Chem. Phys., 25, 12585-12598, 10.5194/acp-25-12585-2025, 2025.

Li, Y., Pöschl, U., and Shiraiwa, M.: Molecular corridors and parameterizations of volatility in the chemical evolution of organic aerosols, Atmos. Chem. Phys., 16, 3327-3344, 10.5194/acp-16-3327-2016, 2016.

Liigand, P., Kaupmees, K., Haav, K., Liigand, J., Leito, I., Girod, M., Antoine, R., and Kruve, A.: Think Negative: Finding the Best Electrospray Ionization/MS Mode for Your Analyte, Analytical Chemistry, 89, 5665-5668, 10.1021/acs.analchem.7b00096, 2017.

Lin, P., Rincon, A. G., Kalberer, M., and Yu, J. Z.: Elemental Composition of HULIS in the Pearl River Delta Region, China: Results Inferred from Positive and Negative Electrospray High Resolution Mass Spectrometric Data, Environmental Science & Technology, 46, 7454-7462, 10.1021/es300285d, 2012.

Mazzoleni, L. R., Saranjampour, P., Dalbec, M. M., Samburova, V., Hallar, A. G., Zielinska, B., Lowenthal, D. H., and Kohl, S.: Identification of water-soluble organic carbon in non-urban aerosols using ultrahigh-resolution FT-ICR mass spectrometry: organic anions, Environ Chem, 9, 285-297, 10.1071/En11167, 2012.

Melendez-Perez, J. J., Martínez-Mejía, M. J., Barcellos, R. L., Fetter-Filho, A. F. H., and Eberlin, M. N.: A potential formation route for CHOS compounds in dissolved organic matter, Marine Chemistry, 202, 67-72, https://doi.org/10.1016/j.marchem.2018.03.006, 2018.

Mohr, C., Lopez-Hilfiker, F. D., Zotter, P., Prévôt, A. S. H., Xu, L., Ng, N. L., Herndon, S. C., Williams, L. R., Franklin, J. P., Zahniser, M. S., Worsnop, D. R., Knighton, W. B., Aiken, A. C., Gorkowski, K. J., Dubey, M. K., Allan, J. D., and Thornton, J. A.: Contribution of Nitrated Phenols to Wood Burning Brown Carbon Light Absorption in Detling, United Kingdom during Winter Time, Environmental Science &

https://doi.org/10.5194/egusphere-2026-4499
Preprint. Discussion started: 1 September 2026

Technology, 47, 6316-6324, 10.1021/es400683v, 2013.
Moise, T., Flores, J. M., and Rudich, Y.: Optical Properties of Secondary Organic Aerosols and Their Changes by Chemical Processes, Chemical Reviews, 115, 4400-4439, 10.1021/cr5005259, 2015.
Myriokefalitakis, S., Vignati, E., Tsigaridis, K., Papadimas, C., Sciare, J., Mihalopoulos, N., Facchini, M. C., Rinaldi, M., Dentener, F. J., Ceburnis, D., Hatzianastasiou, N., O'Dowd, C. D., van Weele, M., and Kanakidou, M.: Global Modeling of the Oceanic Source of Organic Aerosols, Advances in Meteorology, 2010, Artn 939171
10.1155/2010/939171, 2010.
Nair, V. S., Ajith, T. C., Jayachandran, V., Kompalli, S. K., Gogoi, M. M., and Babu, S. S.: Effects of South Asian outflow on aerosol hygroscopicity and cloud droplet activation over the northern Indian Ocean, Atmos Environ, 327, 120500, https://doi.org/10.1016/j.atmosenv.2024.120500, 2024.
Ng, N. L., Brown, S. S., Archibald, A. T., Atlas, E., Cohen, R. C., Crowley, J. N., Day, D. A., Donahue, N. M., Fry, J. L., Fuchs, H. J. A. c., and physics: Nitrate radicals and biogenic volatile organic compounds: oxidation, mechanisms, and organic aerosol, 17, 2103-2162, 2017.
O'Dowd, C. D. and De Leeuw, G.: Marine aerosol production: a review of the current knowledge, Philos T R Soc A, 365, 1753-1774, 10.1098/rsta.2007.2043, 2007.
O'Dowd, C. D., Facchini, M. C., Cavalli, F., Ceburnis, D., Mircea, M., Decesari, S., Fuzzi, S., Yoon, Y. J., and Putaud, J. P.: Biogenically driven organic contribution to marine aerosol, Nature, 431, 676-680, 10.1038/nature02959, 2004.
Ovadnevaite, J., O'Dowd, C., Dall'Osto, M., Ceburnis, D., Worsnop, D. R., and Berresheim, H.: Detecting high contributions of primary organic matter to marine aerosol: A case study, Geophysical Research Letters, 38, Artn L02807
10.1029/2010gl046083, 2011.
Pavuluri, C. M., Kawamura, K., Mihalopoulos, N., and Swaminathan, T.: Laboratory photochemical processing of aqueous aerosols: formation and degradation of dicarboxylic acids, oxocarboxylic acids and α-dicarbonyls, Atmos. Chem. Phys., 15, 7999-8012, 10.5194/acp-15-7999-2015, 2015.
Rejano, F., Casans, A., Via, M., Casquero-Vera, J. A., Castillo, S., Lyamani, H., Cazorla, A., Andrews, E., Pérez-Ramírez, D., Alastuey, A., Gómez-Moreno, F. J., Alados-Arboledas, L., Olmo, F. J., and Titos, G.: CCN estimations at a high-altitude remote site: role of organic aerosol variability and hygroscopicity, EGUsphere, 2024, 1-39, 10.5194/egusphere-2024-1059, 2024.
Rincón, A. G., Calvo, A. I., Dietzel, M., and Kalberer, M.: Seasonal differences of urban organic aerosol composition - an ultra-high resolution mass spectrometry study, Environ Chem, 9, 298-319, 10.1071/En12016, 2012.
Röhrl, A. and Lammel, G.: Determination of malic acid and other C4 dicarboxylic acids in atmospheric aerosol samples, Chemosphere, 46, 1195-1199, https://doi.org/10.1016/S0045-6535(01)00243-0, 2002.
Rosenfeld, D., Zhu, Y., Wang, M., Zheng, Y., Goren, T., and Yu, S.: Aerosol-driven droplet concentrations dominate coverage and water of oceanic low-level clouds, Science, 363, eaav0566, doi:10.1126/science.aav0566, 2019.
Russell, L. M., Hawkins, L. N., Frossard, A. A., Quinn, P. K., and Bates, T. S.: Carbohydrate-like composition of submicron atmospheric particles and their production from ocean bubble bursting, P Natl Acad Sci USA, 107, 6652-6657, 10.1073/pnas.0908905107, 2010.
Sandström, H., Rissanen, M., Rousu, J., and Rinke, P.: Data-Driven Compound Identification in Atmospheric Mass Spectrometry, Adv Sci, 11, 10.1002/advs.202306235, 2024.
Schmeltz, I. and Hoffmann, D.: Nitrogen-containing compounds in tobacco and tobacco smoke,

https://doi.org/10.5194/egusphere-2026-4499
Preprint. Discussion started: 1 September 2026

Chemical Reviews, 77, 295-311, 1977.
Sharmin, T., Monirul Hasan, C. M., Aftabuddin, S., Rahman, M. A., and Khan, M.: Growth, Fatty Acid, and Lipid Composition of Marine Microalgae Skeletonema costatum Available in Bangladesh Coast: Consideration as Biodiesel Feedstock, Journal of Marine Sciences, 2016, 6832847, https://doi.org/10.1155/2016/6832847, 2016.
Shiraiwa, M., Berkemeier, T., Schilling-Fahnestock, K. A., Seinfeld, J. H., and Pöschl, U.: Molecular corridors and kinetic regimes in the multiphase chemical evolution of secondary organic aerosol, Atmos. Chem. Phys., 14, 8323-8341, 10.5194/acp-14-8323-2014, 2014.
Siegel, K., Neuberger, A., Karlsson, L., Zieger, P., Mattsson, F., Duplessis, P., Dada, L., Daellenbach, K., Schmale, J., Baccarini, A., Krejci, R., Svenningsson, B., Chang, R., Ekman, A. M. L., Riipinen, I., and Mohr, C.: Using Novel Molecular-Level Chemical Composition Observations of High Arctic Organic Aerosol for Predictions of Cloud Condensation Nuclei, Environmental Science & Technology, 56, 13888-13899, 10.1021/acs.est.2c02162, 2022.
Song, J., Li, M., Jiang, B., Wei, S., Fan, X., and Peng, P. a.: Molecular Characterization of Water-Soluble Humic like Substances in Smoke Particles Emitted from Combustion of Biomass Materials and Coal Using Ultrahigh-Resolution Electrospray Ionization Fourier Transform Ion Cyclotron Resonance Mass Spectrometry, Environmental Science & Technology, 52, 2575-2585, 10.1021/acs.est.7b06126, 2018.
Song, J., Li, M., Fan, X., Zou, C., Zhu, M., Jiang, B., Yu, Z., Jia, W., Liao, Y., and Peng, P. a.: Molecular Characterization of Water- and Methanol-Soluble Organic Compounds Emitted from Residential Coal Combustion Using Ultrahigh-Resolution Electrospray Ionization Fourier Transform Ion Cyclotron Resonance Mass Spectrometry, Environmental Science & Technology, 53, 13607-13617, 10.1021/acs.est.9b04331, 2019.
Sun, H., Wu, Z., Kang, X., Zhu, C., Yu, L., Li, R., Lin, Z., and Chen, J.: Molecular characterization of humic-like substances (HULIS) in atmospheric particles (PM2.5) in offshore Eastern China Sea (OECS) using solid-phase extraction coupled with ESI FT-ICR MS, Atmospheric Environment, 294, 119523, https://doi.org/10.1016/j.atmosenv.2022.119523, 2023.
Sun, H., Li, X., Zhu, C., Huo, Y., Zhu, Z., Wei, Y., Yao, L., Xiao, H., and Chen, J.: Molecular composition and optical property of humic-like substances (HULIS) in winter-time PM2.5 in the rural area of North China Plain, Atmospheric Environment, 252, 118316, https://doi.org/10.1016/j.atmosenv.2021.118316, 2021.
Tang, J., Li, J., Su, T., Han, Y., Mo, Y., Jiang, H., Cui, M., Jiang, B., Chen, Y., Tang, J., Song, J., Peng, P., and Zhang, G.: Molecular compositions and optical properties of dissolved brown carbon in biomass burning, coal combustion, and vehicle emission aerosols illuminated by excitation–emission matrix spectroscopy and Fourier transform ion cyclotron resonance mass spectrometry analysis, Atmos. Chem. Phys., 20, 2513-2532, 10.5194/acp-20-2513-2020, 2020.
Tao, S., Lu, X., Levac, N., Bateman, A. P., Nguyen, T. B., Bones, D. L., Nizkorodov, S. A., Laskin, J., Laskin, A., and Yang, X.: Molecular Characterization of Organosulfates in Organic Aerosols from Shanghai and Los Angeles Urban Areas by Nanospray-Desorption Electrospray Ionization High-Resolution Mass Spectrometry, Environmental Science & Technology, 48, 10993-11001, 10.1021/es5024674, 2014.
Tian, M., Li, H., Wang, G., Fu, M., Qin, X., Lu, D., Liu, C., Zhu, Y., Luo, X., Deng, C., Abdullaev, S. F., and Huang, K.: Seasonal source identification and formation processes of marine particulate water soluble organic nitrogen over an offshore island in the East China Sea, Sci Total Environ, 863, 160895, https://doi.org/10.1016/j.scitotenv.2022.160895, 2023.

https://doi.org/10.5194/egusphere-2026-4499
Preprint. Discussion started: 1 September 2026

Tröstl, J., Chuang, W. K., Gordon, H., Heinritzi, M., Yan, C., Molteni, U., Ahlm, L., Frege, C., Bianchi, F., Wagner, R., Simon, M., Lehtipalo, K., Williamson, C., Craven, J. S., Duplissy, J., Adamov, A., Almeida, J., Bernhammer, A. K., Breitenlechner, M., Brilke, S., Dias, A., Ehrhart, S., Flagan, R. C., Franchin, A., Fuchs, C., Guida, R., Gysel, M., Hansel, A., Hoyle, C. R., Jokinen, T., Junninen, H., Kangasluoma, J., Keskinen, H., Kim, J., Krapf, M., Kürten, A., Laaksonen, A., Lawler, M., Leiminger, M., Mathot, S., Möhler, O., Nieminen, T., Onnela, A., Petäjä, T., Piel, F. M., Miettinen, P., Rissanen, M. P., Rondo, L., Sarnela, N., Schobesberger, S., Sengupta, K., Sipilä, M., Smith, J. N., Steiner, G., Tomè, A., Virtanen, A., Wagner, A. C., Weingartner, E., Wimmer, D., Winkler, P. M., Ye, P. L., Carslaw, K. S., Curtius, J., Dommen, J., Kirkby, J., Kulmala, M., Riipinen, I., Worsnop, D. R., Donahue, N. M., and Baltensperger, U.: The role of low-volatility organic compounds in initial particle growth in the atmosphere, Nature, 533, 527-+, 10.1038/nature18271, 2016.

van Pinxteren, M., Fiedler, B., van Pinxteren, D., Iinuma, Y., Körtzinger, A., and Herrmann, H.: Chemical characterization of sub-micrometer aerosol particles in the tropical Atlantic Ocean: marine and biomass burning influences, J Atmos Chem, 72, 105-125, 10.1007/s10874-015-9307-3, 2015.

Wan, Y. B., Huang, X. P., Ge, X. L., Jiang, B., Liao, Y. H., Yan, Q., Shuai, Q., Fu, Q. L., Xiao, H., and Yu, H.: Size-dependent Molecular Characteristics and Possible Sources of Organic Aerosols at a Coastal New Particle Formation Hotspot of East China, J Geophys Res-Atmos, 126, ARTN e2021JD034610 10.1029/2021JD034610, 2021.

Wan, Y. B., Huang, X. P., Jiang, B., Kuang, B. Y., Lin, M. F., Xia, D. M., Liao, Y. H., Chen, J. W., Yu, J. Z., and Yu, H.: Probing key organic substances driving new particle growth initiated by iodine nucleation in coastal atmosphere, Atmos Chem Phys, 20, 9821-9835, 10.5194/acp-20-9821-2020, 2020.

Wang, J., Chen, J., Qiao, X., Wang, Y., Cai, X., Zhou, C., Zhang, Y., and Ding, G.: DOM from mariculture ponds exhibits higher reactivity on photodegradation of sulfonamide antibiotics than from offshore seawaters, Water Research, 144, 365-372, https://doi.org/10.1016/j.watres.2018.07.043, 2018a.

Wang, K., Zhang, Y., Huang, R. J., Cao, J. J., and Hoffman, T.: UHPLC-Orbitrap mass spectrometric characterization of organic aerosol from a central European city (Mainz, Germany) and a Chinese megacity (Beijing), Atmospheric Environment, 189, 22-29, 10.1016/j.atmosenv.2018.06.036, 2018b.

Wang, K., Zhang, Y., Tong, H., Han, J., Fu, P., Huang, R.-J., Zhang, H., and Hoffmann, T.: Molecular-Level Insights into the Relationship between Volatility of Organic Aerosol Constituents and PM2.5 Air Pollution Levels: A Study with Ultrahigh-Resolution Mass Spectrometry, Environmental Science & Technology, 58, 7947-7957, 10.1021/acs.est.3c10662, 2024.

Wang, K., Huang, R. J., Brüggemand, M., Zhang, Y., Yang, L., Ni, H. Y., Guo, J., Wang, M., Han, J. J., Bilde, M., Glasius, M., and Hoffmann, T.: Urban organic aerosol composition in eastern China differs from north to south: molecular insight from a liquid chromatography-mass spectrometry (Orbitrap) study, Atmospheric Chemistry and Physics, 21, 9089-9104, 10.5194/acp-21-9089-2021, 2021.

Wang, X., Hayeck, N., Brüggemann, M., Yao, L., Chen, H., Zhang, C., Emmelin, C., Chen, J., George, C., and Wang, L.: Chemical Characteristics of Organic Aerosols in Shanghai: A Study by Ultrahigh-Performance Liquid Chromatography Coupled With Orbitrap Mass Spectrometry, Journal of Geophysical Research: Atmospheres, 122, 11,703-711,722, https://doi.org/10.1002/2017JD026930, 2017.

Wang, X. K., Rossignol, S., Ma, Y., Yao, L., Wang, M. Y., Chen, J. M., George, C., and Wang, L.: Molecular characterization of atmospheric particulate organosulfates in three megacities at the middle and lower reaches of the Yangtze River, Atmos. Chem. Phys., 16, 2285-2298, 10.5194/acp-16-2285-2016, 2016.

https://doi.org/10.5194/egusphere-2026-4499
Preprint. Discussion started: 1 September 2026

Wang, Y., Xie, R., Shen, Y., Cai, R., He, C., Chen, Q., Guo, W., Shi, Q., Jiao, N., and Zheng, Q.: Linking Microbial Population Succession and DOM Molecular Changes in Synechococcus-Derived Organic Matter Addition Incubation, Microbiology Spectrum, 10, e02308-02321, doi:10.1128/spectrum.02308-21, 2022.

Wang, Y., Hu, M., Wang, Y., Zheng, J., Shang, D., Yang, Y., Liu, Y., Li, X., Tang, R., Zhu, W., Du, Z., Wu, Y., Guo, S., Wu, Z., Lou, S., Hallquist, M., and Yu, J. Z.: The formation of nitro-aromatic compounds under high NOx and anthropogenic VOC conditions in urban Beijing, China, Atmos. Chem. Phys., 19, 7649-7665, 10.5194/acp-19-7649-2019, 2019.

Wang, Y., Zhang, Y., Li, W., Wu, G., Qi, Y., Li, S., Zhu, W., Yu, J. Z., Yu, X., Zhang, H.-H., Sun, J., Wang, W., Sheng, L., Yao, X., Gao, H., Huang, C., Ma, Y., and Zhou, Y.: Important Roles and Formation of Atmospheric Organosulfates in Marine Organic Aerosols: Influence of Phytoplankton Emissions and Anthropogenic Pollutants, Environmental Science & Technology, 57, 10284-10294, 10.1021/acs.est.3c01422, 2023.

Weng, H., Lin, J., Martin, R., Millet, D. B., Jaegle, L., Ridley, D., Keller, C., Li, C., Du, M., and Meng, J.: Global high-resolution emissions of soil NO(x), sea salt aerosols, and biogenic volatile organic compounds, Sci Data, 7, 148, 10.1038/s41597-020-0488-5, 2020.

Willoughby, A. S., Wozniak, A. S., and Hatcher, P. G.: A molecular-level approach for characterizing water-insoluble components of ambient organic aerosol particulates using ultrahigh-resolution mass spectrometry, Atmospheric Chemistry and Physics, 14, 10299-10314, 10.5194/acp-14-10299-2014, 2014.

Wozniak, A. S., Willoughby, A. S., Gurganus, S. C., and Hatcher, P. G.: Distinguishing molecular characteristics of aerosol water soluble organic matter from the 2011 trans-North Atlantic US GEOTRACES cruise, Atmos. Chem. Phys., 14, 8419-8434, 10.5194/acp-14-8419-2014, 2014.

Wu, S., Fujii, M., and Fu, Q.: Molecular characterization of coastal seawater dissolved organic matter by ultrahigh-resolution mass spectrometry: a photochemical study of the Tokyo Bay, Japan, Carbon Research, 2, 46, 10.1007/s44246-023-00083-z, 2023.

Xu, W., Chen, C., Qiu, Y., Li, Y., Zhang, Z., Karnezi, E., Pandis, S. N., Xie, C., Li, Z., Sun, J., Ma, N., Xu, W., Fu, P., Wang, Z., Zhu, J., Worsnop, D. R., Ng, N. L., and Sun, Y.: Organic aerosol volatility and viscosity in the North China Plain: contrast between summer and winter, Atmos. Chem. Phys., 21, 5463-5476, 10.5194/acp-21-5463-2021, 2021.

Ye, Y., Zhan, H., Yu, X., Li, J., Wang, X., and Xie, Z.: Detection of organosulfates and nitrooxy-organosulfates in Arctic and Antarctic atmospheric aerosols, using ultra-high resolution FT-ICR mass spectrometry, Sci Total Environ, 767, 144339, https://doi.org/10.1016/j.scitotenv.2020.144339, 2021.

Yu, Z. and Li, Y.: Marine volatile organic compounds and their impacts on marine aerosol-A review, Sci Total Environ, 768, 145054, 10.1016/j.scitotenv.2021.145054, 2021.

Zhang, M., Cai, D., Lin, J., Liu, Z., Li, M., Wang, Y., and Chen, J.: Molecular characterization of atmospheric organic aerosols in typical megacities in China, npj Climate and Atmospheric Science, 7, 230, 10.1038/s41612-024-00784-1, 2024.

Zhang, X., Li, L., Li, J., Lin, Y., Cheng, Y., Wang, R., Xing, S., Zhu, C., Cao, J., and Han, Y.: Influence of anthropogenic pollution on the molecular composition of organic aerosols over a forest site in the Qinling Mountains region of central China, EGUsphere, 2025, 1-24, 10.5194/egusphere-2025-519, 2025.

Zhang, Y., Wang, K., Tong, H., Huang, R.-J., and Hoffmann, T.: The maximum carbonyl ratio (MCR) as a new index for the structural classification of secondary organic aerosol components, Rapid Communications in Mass Spectrometry, 35, e9113, https://doi.org/10.1002/rcm.9113, 2021.

Zhao, Y., Hallar, A. G., and Mazzoleni, L. R.: Atmospheric organic matter in clouds: exact masses and

https://doi.org/10.5194/egusphere-2026-4499
Preprint. Discussion started: 1 September 2026

molecular formula identification using ultrahigh-resolution FT-ICR mass spectrometry, Atmospheric Chemistry and Physics, 13, 12343-12362, 10.5194/acp-13-12343-2013, 2013.

Zhu, Y., Li, H., Xing, C., Dong, X., Liu, C., Qin, X., Wang, G., Liu, Z., Ding, Z., Tian, M., Deng, C., and Huang, K.: Unraveling a Novel Formation Pathway of Hydroxymethanesulfonate (HMS) in the Marine Atmosphere, Journal of Geophysical Research: Atmospheres, 129, e2024JD041936, https://doi.org/10.1029/2024JD041936, 2024.

Zhu, Y., Li, H., Wei, J., Ding, H., Cai, D., Zou, X., Wang, G., Wang, Q., Ding, Z., Liu, Z., Chen, J., Yun, L., Deng, C., and Huang, K.: Marine Modulation of the Formation Pathways and Sources of Organosulfates over the Coastal South China Sea, Environmental Science & Technology Letters, 12, 739-746, 10.1021/acs.estlett.5c00406, 2025.